MICROWAVE COMPONENTS IN THE ECR ALICE AND A MODEL FOR PLASMA IMPEDANCE

M. Cavenago, C.T. Iatrou

MICROWAVE COMPONENTS IN THE ECR ALICE
AND A MODEL FOR PLASMA IMPEDANCE

M.Cavenago, C.T. Iatrou *
Laboratori Nazionali di Legnaro, INFN
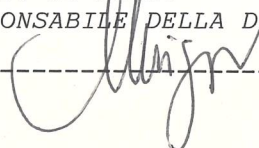via Romea n. 4, I-35020 Legnaro (PD), Italy

The design of the DC-break and the waveguide terminations were improved during the long shutdown of the ECR ion source Alice. The DC-break features a compact dielectric enclosure, a teflon insulator treated by surface ion implantation and a suitably matched choke flange. The correction to the usual choke design due to the finite flange separation and the teflon insulator are discussed, showing that the choke cannot avoid producing a reactive component at the main waveguide position. Proper design of the radial line following the choke is emphasized, determining the outer dimension of the flange. The electrostatic fields and the behaviour of the DC-break are discussed, showing the risks of microwave power transients and proposing the metallization of the insulator sides. Consequent microwave losses are computed, for arbitrary values of the conductivity σ and the conducting layer thickness d_c. Losses are contained to a mere 0.01 % , if $\sigma d_c < 10^{-7}$ mho, which is feasible by ion implantation. The waveguide termination is discussed, showing the separation between antenna reflections, which may be important for a particular antenna design, and the plasma reflections, which seems to be calculable and practically negligible (below 5 %). The directivity properties of slanted cuts are pointed out, and possible choices for a new coupler are discussed, within a simple ray tracing approach. A model for microwave absorption in a strongly collisional plasma is proposed, using Krook's model for electron motion and allowing discussion of inhomogeneous system on wavelength scale λ. Separation in cylindrical coordinate is performed, assuming that the plasma density and the ion source magnetic field B_z^0 are approximated by function of only the source axis z. A scalar mode separation, retrieving left-handed and right-handed waves, is obtained, thanks to the fact that $D/\lambda \cong 3 \gg 1$. An ordinary differential equation for the amplitude of each scalar and transverse mode is found, showing no adiabatic compression of the microwave electric field at ECR resonance. A simple formula for the plasma impedance is obtained, involving sum on modes, and the impedance for each mode is defined. Several cases are tabulated.

I. INTRODUCTION

In ECR ion sources, microwaves are absorbed by the plasma through the Electron Cyclotron Resonance phenomen [1] ; since cavity diameters range from one to three wavelengths and plasma conditions change in a wavelength, non-uniformity effects expected to be important and geometric optics approximations are no longer valid. Anyway, the plasma is good absorber for microwaves. In practice we expect that all the radiated microwave power will be absorbed by the plasma or the cavity wall, and that major reflections may originate only in the antenna or in the previous circuit, shown in Fig. 1 . The observation of a 30-50 % reflection from the second stage circuit of the ion source Alice [2] led us to redesign the DC-break and the waveguide termination inside the plasma, which acts as an antenna.

DC-breaks are traditional components in ECR ion sources, because the klystron amplifier and all other power equipments stay at room potential, while the source vessel is biased to $V_s = 10 \div 20$ kV. DC-breaks differ greatly from microwave windows because no metallic

---

* *Present address: KfK-ITP Karlsruhe, Postfach 3640, D-76021, Karlsruhe, Germany.*

9/3/1994   AUTORIZZO LA PUBBLICAZIONE

PROF. M. NIGRO
RESPONSABILE DELLA DIVISIONE RICERCA

continuity is allowed and power may be radiated, besides being reflected or transmitted. Radiation may be important [3,4,5], as seen by circuit theory or geometric optics consideration, or by solvable models (treated in a separate report [6]). The basic design (of DC-break for ECRs) involves a sheet of dielectric clamped between two microwave flanges [1,7] with some additional cooling [8].

Our previous design was somewhat more complex, mainly for cooling and mechanical reasons (Fig. 2): the goal was to have a completely segmented and demountable DC-break. The observation of erratic electric sparks even at $V_s = 9$ kV when the microwave were on (16 kV when microwave off) and the high mortality of microwave detection diodes leads us to suspect the DC-break as a possible spark origin; consistently with it, we always observe waveguide arcs after the sparks. To reduce risks of sparks in the DC-break, we try to smooth edges and reduce metallic parts as much as possible.

The sharp edges of the waveguide at the flanges (and of the necessary choke) may be electrostatically shielded by modifying the surface conductivity of the insulator, which is a well studied technology in our laboratories (it serves for high energy detectors). In view of the surface resistivity required, ion implantation was chosen [9]; still we will speak of a metal deposit or film, even if actually we have a polymer whose surface conducts. With TOSCA simulation [10] we may show that the greatest disadvantage of non-metallized window is the disuniformity of the electrostatic field, which has also a substantial tangential component at the interface with air, more than the increase in the maximum field intensity (a mere 20 % higher than the metallized one).

In perspective a DC-break with low radiated and reflected power may serve as a basic component for power transmission to a 200 kV biased permanent magnet ECR ion source aimed at producing high current ion beams.

II. DC-BREAK DESIGN; NECESSITY OF A CHOKE

A DC-break needs a dielectric sheet of thickness d ; since reliability of the insulation is the first concern, we took $d = 1$ mm, even if thinner foils may stand the stated voltage ($V_s = 10 \div 20$ kV) at least for short periods. More than the foil thickness, it is important that surface discharge path to be as long as possible, which is easily accomplished by large diameter disks. The disk constitutes a radial waveguide, through which power may escape.

A sketch of the current on the guide walls shows immediately the physical reason of the radiated wave (Fig. 3). Let z be the guide direction, a and b the minor and major sides of the rectangular waveguide section and the axis x parallel to the major side. In the fundamental TE_{10} mode, we excite the field:

$$B_z = B_0 \cos(\pi x/b)e^{ik_g z - i\omega t} \qquad E_y = i(\omega b/\pi)B_0 \sin(\pi x/b)e^{ik_g z - i\omega t} \qquad B_x = -(k_g/\omega)E_y \tag{1}$$

for $0 \le x \le b$ and $0 \le y \le a$; here $k_g = \sqrt{(\omega/c)^2 - (\pi/b)^2}$ is the guided wavenumber and $\omega/2\pi = 14.4$ GHz the microwave frequency. The wall currents are given by $\mathbf{j} = \mathbf{H} \wedge \mathbf{n}$, where $\mathbf{n}$ is the inward normal to the wall; on the major sides of the waveguide, we find

$$j_z = \mp i(kbB_0/\pi\mu_0)\sin(\pi x/b)e^{ik_g z - i\omega t} \qquad j_x = \pm(B_0/\mu_0)\cos(\pi x/b)e^{ik_g z - i\omega t} \tag{2}$$

where the upper sign applies to the upper major side and the lower sign to the lower side. At the cut, the j_z current has to bend in the y direction, thus originating a radiation at the upper and lower side; the j_x component flows parallel to the cut, and closes on the lateral sides. On the minor sides we indeed find only a j_y component.

2

This suggests that a first estimate of the radiated power may be obtained by assuming no wave diffraction in the x direction, that is to say that the field will be of the form

$$f(x, y, z, t) = f(y, z) \exp(-i\omega t + ik_b x) \tag{3}$$

with $k_b = \pi/b$. Pictorially, this is obtained by removing the walls at $x = 0$ and $x = b$ and extending the remaining walls to $-\infty$ and to $+\infty$ in x ; since we impose the factor $\exp(i\pi x/b)$ we can still obtain zero E_y field at the removed walls, consistently with the actual device conditions; we call it the "four guide model".

II.A) *Circuit analysis of the four guide junction*

Analytic evaluation of the four guide model is possible and is covered in a separate paper [6]. The radiated power agrees with results of the much simpler circuit analysis[11], which is directly applicable to a four guide model; the schematic of it is given in Fig. 4 , where only arms labelled "in","out",1 and 1′ are considered and they are extended to infinity.

Even if a waveguide has no two poles like a transmission line, still we can speak of the voltage, of the total forward current (on upper side) and of the total forward power transmitted through a waveguide excited with a given mode propagating forward, and we can therefore define the (characteristic) mode impedance (we avoid the phrase 'characteristic impedance' alone because sometimes it is used with other meanings). In detail, for the TE_{10} mode, the power, the local voltage and the current are

$$P(z, t) = \int \mathrm{d}x\mathrm{d}y \, E_y H_x \tag{4}$$

$$\tilde{V}(x, z, t) = \int_0^a \mathrm{d}y \, E_y \qquad I(z, t) = \int_0^b \mathrm{d}x \, H_x \tag{5}$$

where the local voltage $\tilde{V}$ has a sinusoidal dependence on x . The value of it at a given value of x , determined with some arbitrary but resonable choice, is to be taken as the definition of voltage V; here we choose to define V as $V = P/I$ according to usual lumped circuit formula.

We define the characteristic mode impedance as $Z_o = V/I$. We get by straightforward integration

$$Z_o(a, b, \epsilon) = Z_w \frac{a}{b} \frac{\pi^2}{8} \quad \text{where} \quad Z_w = \sqrt{\frac{\mu}{\epsilon}} \frac{1}{\sqrt{1 - (\pi c/b\omega)^2}} \tag{6}$$

is the "wave impedance" for the mode, the frequency and the waveguide given. Note that only the last factor $\pi^2/8 \cong 1$ of Z_o depends on the particular choice $\tilde{V}$ averaging. For the standard WR62 waveguide (alias R140; defined by $a = 0.79$ cm and $b = 1.58$ cm) at 14.4 GHz we have $Z_w = 501$ ohm and $Z_o(a, b, 1) = 309$ ohm.

We assume that the output port load is matched, so that no backward wave propagates for $z > d$. The impedance of the arm "out" is then the mode impedance $Z_{out} = Z_o(a, b, 1)$ from Eq. (6) . Here the dielectric filled arms 1 and 1′are matched because they are infinitely long (physically wave dies out because of unavoidable absorption before reaching $y = \pm\infty$); their impedance $Z_1 = Z_{1'} = Z_o(w_c, b, \epsilon)$ is proportional to w_c as given by (6) and real. In the actual choke, Z_1 is generally complex, while Z_{out} is real.

While the port "in" itself has a mode impedance $Z_{in} = Z_{out}$, the impedance presented against this port "in" is $Z_t = Z_{out} + 2Z_1$, assuming negligible edge and junction effects (no

3

phase delay between ports). Ports "out ",1 and 1'are in series because the current emitted from "in " flows in each of them, while the power shares.

The reflection ρ, transmission τ and leakage L (per port) coefficients may be computed, by the well-known circuit analysis and by considering that power distributes into the 1 and "out" ports proportionally to their impedance $L : T = \Re[Z_1] : Z_{out}$. We find

$$\rho = \left| \frac{Z_t - Z_{out}}{Z_t + Z_{out}} \right|^2 = \left| \frac{Z_1}{Z_{out} + Z_1} \right|^2 \tag{7}$$

$$T = \left| \frac{2Z_{out}}{Z_t + Z_{out}} \right|^2 = \frac{Z_{out}^2}{|Z_{out} + Z_1|^2} \tag{8}$$

$$L = \frac{\Re[Z_1]}{Z_{out}} \left| \frac{2Z_{out}}{Z_t + Z_{out}} \right|^2 = \frac{Z_{out} \Re[Z_1]}{|Z_1 + Z_{out}|^2} \tag{9}$$

Note that $\rho + \tau + 2L = 1$. From the values of Z_{out} and Z_1 given by Eq. (6) , after taking w_c equal to the minimal flanges separation $w_c = d$, the total radiated power is

$$2L = 2\sqrt{\epsilon_r}da/(d + \sqrt{\epsilon_r}a)^2 \qquad :$$

microwaves escape much better than water will do when it flows in the same copper tube.

II.B) *The choke principle*

The preceeding argument gives only the magnitude of the radiation and evidences the necessity of a corrective action, namely a choke flange; the fact that our DC-break cannot have yz walls prevent us to use the choke geometry corresponding to the four guide model, that is the so called British choke; this choke is also suited for exact computation [3]. The old DC-break actually used a standard choke, and was successful in avoiding large radiation.

Our choke should resemble the standard choke, which is based on an approximate azimuthal symmetry, discussed in the following. The standard choke assumes touching flanges and the determination of the parameters w_c (choke spacing, typically 0.2 mm), w_g (groove width), d_g (groove height) and R_g (groove mean radius) is partly analytical and partly empirical; we consider here that the lower bound for w_c and the dielectric presence ($\epsilon \neq 1$) compel us to review the other parameters; we add two parameters, namely the spacing between flanges w_t (which is zero in standard choke) and the outer flange radius R_o (Fig. 4).

The principle and the basic calculation of these chokes are better understood with the four guide model (see Fig. 5 for symbols), while azimuthally symmetric model is suitable for further corrections. In the choke, the port 1 is constituted by a radial line 1, branching into a coaxial line 'g' carved into the metallic body of one flange and a radial line 2, terminating into the open space.

The input impedance Z_1^i at the junction with the main waveguide is the transformation, which is caused by the line 1 with mode impedance $Z_1^o = Z_o(w_c, b, \epsilon)$, of the load impedance Z_1^l :

$$Z_1^i = Z_1^o \frac{Z_1^l - iZ_1^o \tan \beta_1}{-iZ_1^l \tan \beta_1 + Z_1^o} \tag{10}$$

where β_1 is the phase length of the line 1 given by $\beta_1 = \lambda_1(R_g + \frac{1}{2}w_g - \frac{1}{2}a) + O(w_c + w_g/\lambda_1)$, with the line 1 wavelength $\lambda_1 = \lambda/\sqrt{1 - (\pi c/\omega b)^2}$. By taking $\beta_1 \cong \pi/2$ and Z_1^l as large as possible we can minimize Z_1^i , which minimizes both reflection and radiation losses.

4

In turn, the former impedance Z_1^l is given by $Z_1^l = Z_g^i + Z_2^i$, since the groove and the line 2 are in series; by taking the branching ratio Z_g^i/Z_2^i as large as possible we can reduce further the radiation (obtaining some more reflection); indeed we direct more of the line 1 power in the groove than in the leaking line 2 . Since the groove is reliably short-circuited by bulk metal at one end, the impedance at the other end is

$$Z_g^i = -iZ_g^o \tan \beta_g \qquad (11)$$

where $Z_g^o \cong Z_o(w_g, b, 1)$ is the coaxial mode impedance of the groove and $\beta_g = 2\pi/\lambda_g$; here $\lambda_g = \lambda_g(1)$ is the guided wavelength of the coaxial guide mode TE_{10} , which is the mode mainly excited in the groove and can be evaluated from the formula valid for TE_{n0} modes:

$$\lambda_g(n) = \frac{(2\pi c/\omega)}{\sqrt{1 - (2\pi n/C\omega)}} \qquad (12)$$

where C is the average circumference of the groove.

At the nominal frequency, by taking $\beta_g = \pi/2$, the impedance Z_g^i becomes infinite and therefore the radiation vanishes, notwithstanding the presence of a finite second line impedance Z_2^i . The choke principle thus consists in inserting the imperfect contact represented by line 2 impedance in the current node of a perfectly shorted line (the groove plus the line 1).

Ideally, the condition $\beta_g = \pi/2$ is sufficient to suppress any radiation. Since frequency variation, machining errors and correction to line transmission circuit theory (due to classical field theory) still need to be care of, it is anyway advisable to make Z_g^o much greater than Z_1^o (to further enhance Z_g^i) and Z_2^i as small as possible. In particular, Z_2^i is given by a formula completely similar to eqn. (10) as:

$$Z_2^i = Z_2^o \frac{Z_2^l - iZ_2^o \tan \beta_2}{-iZ_2^l \tan \beta_2 + Z_2^o} \qquad (13)$$

where the phase length of line 2 is $\beta_2 = 2\pi(R_o + \frac{1}{2}r_r - (r_e + \frac{1}{2}w_c))/\lambda_1$ and Z_2^l is the impedance at the end of the line 2; this end consists of two smoothed facing edges and therefore acts as an antenna.

Note that we desire a bad antenna, that is Z_2^l as high as possible, to this purpose exploiting the mismatch between the relatively high vacuum space impedance ($Z_v = 377$ Ohm per square) and the low radial line impedance (slowly changing with r):

$$Z_2^o(r) = \frac{Z_v w_t}{2\pi r\sqrt{\epsilon_r}} = 2 \qquad \text{Ohm at} \qquad r = R_o \qquad (14)$$

Since a tapered horn will produce the undesired matching of the vacuum impedance to line 2 (and therefore $Z_2^l \cong Z_2^o(R_o)$), we made the edges as sharp as compatible with electrostatic field limitation, requiring that $r_r \ll \lambda/2$. A good design value seemed $r_r = 3$ mm. We can then consider the antenna impedance, estimated as $Z_v\lambda/R_o$ (which is much greater than Z_o) as directly connected to the line 2, therefore obtaining $Z_2^l = Z_v\lambda/R_o$, so that line 2

5

termination approximates an open line condition ($Z_2^l \gg Z_2^o$). The same argument used in eq. (10) proves that, by taking $\beta_2 = \pi/2$ in eq. (13), we can produce an impedance as low

$$Z_2^i = (Z_2^o)^2 / Z_2^l \tag{15}$$

at the other line 2 termination. We conclude that Z_2^i can be made real and much smaller than $Z_2^o(R_g)$, and we indicate its value by $R = Z_2^i$; from eqs. (14) and (15) a very rough estimate (depending on antenna design) is:

$$R \cong Z_o(R_g) \frac{w_t}{\lambda} \tag{16}$$

whose uncertainties cover all design and machining errors in line 2 parameters by far.

From previous eqs. (10), (11) and (13), we can precisely determine the effect on Z_1^i of variations (due both to frequency change and construction tolerances) of β_1 and β_g from their nominal value $\pi/2$; let us define

$$\delta_1 = \beta_1 - \pi/2 \ll \pi/2 \qquad \delta_g = \beta_g - \pi/2 \ll \pi/2 \tag{17}$$

Note that β_g can be easily computed from coaxial line, while β_1 requires actually to consider a radial propagation, so that a theoretical error is likewise included in δ_1. Moreover, let us anticipate that we can not choose by design $\beta_1 = \pi/2$ for practical reasons explained in section II.C. Standard propagation of errors in eq. (10) -(13) gives:

$$Z_1^i = -iZ_1^o \left\{ \delta_1 \left(1 + \frac{Z_1^o}{Z_g^o} \right) + iR \frac{Z_1^o}{Z_g^{o\,2}} \delta_g^2 \right\} \tag{18}$$

This expression compares and summarizes the respective merits of the five design points: i) making Z_1^o smaller (that implies the reduction of d); ii) making Z_g^o higher; iii) making δ_1 near to zero; iv) making δ_2 to vanish; v) reducing R by a careful line 2 termination. For example, in order to make the resistive part R_1^i of Z_1^i much lower ($<\ 10^{-3}$ times) than R, moderate tolerances on the groove widths ($\delta_g < 0.1$) and feasible groove widths are required: $w_g/w_c = 2.5$ so that $Z_1^o/Z_g^1 = 4$; no quantitative condition is necessary for δ_1 but the statement in Eq. (18). The radiation coefficient is

$$L = \left| \frac{Z_{\text{out}}}{Z_{\text{out}} + Z_1^i} \right|^2 \frac{R_1^i}{Z_{\text{out}}} \tag{19}$$

from eq. (9) and it may be globally reduced to $<\ 10^{-6}$.

The reactance X_1^i is instead proportional to δ_1, but it enters anyway squared into the reflection coefficient of eq. (7);

$$\rho \cong \frac{X_1^{i\,2} + R_1^{i\,2}}{|Z_{\text{out}}|^2} \tag{20}$$

6

II.C) *The azimuthal symmetry and the actual design of a choke.*

Another approximation for transmission calculations in the gap between flanges comes from considering that the j_z current (see eq. (2)) may be projected onto an approximate $\cos(\vartheta)$ distribution on some imaginary circular wave guide section of effective radius r_e ; for the azimuthal symmetry of this model the radiated wave may be computed exactly. This model is thus useful in determining groove position and effects, provided that the indeterminacy in r_e is fixed. From empirical consideration and comparison with standard choke flanges we take

$$r_e = \tfrac{1}{4}(a+b) \tag{21}$$

The impedance transformation law for a radial line from radius r_i to radius r_l is

$$Z_i = Z_o(r_i)\frac{Z_l\mathrm{Ct}(x,y) - iZ_o(r_l)\zeta(x,y)}{-iZ_o(r_l)\zeta(x,y)\mathrm{ct}(x,y) + Z_l} \tag{22}$$

where Z_i and Z_l are the impedance at the two ends, $x = \sqrt{\epsilon_r}\omega r_i/c$ and $y = \sqrt{\epsilon_r}\omega r_l/c$ are dimensionless coordinates representing the line extrema and the functions are related to Bessel function J and N by

$$\mathrm{ct}(x,y) = \frac{J_1(x)N_0(y) - N_1(x)J_0(y)}{J_0(x)N_0(y) - N_0(x)J_0(y)} \tag{23}$$

$$\mathrm{Ct}(x,y) = -\frac{J_0(x)N_1(y) - N_0(x)J_1(y)}{J_1(x)N_1(y) - N_1(x)J_1(y)} \tag{24}$$

$$\zeta(x,y) = \frac{J_0(x)N_0(y) - N_0(x)J_0(y)}{J_1(x)N_1(y) - N_1(x)J_1(y)} \tag{25}$$

To follow the four guide model choke design, we set $Z_i = 0$, $Z_l = \infty$ (corresponding to a $\pi/2$ phase length in linear guides) and $r_i = r_e$ in the above equations; we then find that their lower solution $r_l = r_1$ is $r_l = 9.207$ mm when $\epsilon_r = 2.1$ (Teflon). This radius is smaller than the standard groove radius, because the same dimensionless coordinate y correspond to smaller and smaller physical radii, the larger ϵ_r is.

Actually that groove will cut the waveguide, so we exclude $R_g = 9.207$ mm. We choose $R_g = 10.5$ mm as the lowest feasible and reasonable value. Setting $r_l = R_g$ and $Z_l = \infty$ in eq. (22) -(25) we find $Z_i = -i4$ Ohm at $r_i = r_e$, which is small compared to $Z_{\mathrm{out}} = 309$ Ohm. From eq. (20) , we find the reflection $\rho = 0.0001$, which is tolerable and indeed shows that δ_1 effects are small.

In that condition, we proved that leakage radiation depends only on δ_g , that is on groove depth, where no radial correction is needed. From β_g expression for coaxial line, still valid, we find $d_g = 5.48$ mm.

It can be argued that r_e is somewhat arbitrary and therefore the smallness of Z_i need to be verified at different radii. In particular, since j_z has its peak values at $y = b/2$ (in the middle points of the major sides), the case for $r_i = a/2 = 3.95$ mm needs to be checked. We find $Z_i = 24.4$ Ohm, still giving a tolerable reflection $\rho = 0.002$.

Two conclusive comments may be said on the groove profile in xy plane. The fact that groove radius r_1 cuts the waveguide proves that azimuthal symmetry is greatly perturbed (at the groove) by the rectangular waveguide, and therefore, the exact groove path will not be a circumference. Anyway, we showed that a larger circumference will give only reflection,

7

but not leakage, so we follow the usual choice of a circumference for reason of machining with a simple lathe.

It was observed that half-millimeter flange misalignment in x and/or y may ruin choke operation; the reason is that coaxial mode TE30 may propagate in the groove, with different wavelength λ'_g , if this mode is excited by misalignments [3]. One remedy is to fill the circle portion near to the minor sides. This is the so-called plugged groove. Minor changes result in TE10 wavelength, obtaining $d_g = 5.8$ mm. We avoid this complication in the present design, also because the interaction between plugged groove and dielectric sheets needs further investigation. The present design therefore envisions a robust centering plastic case (see Fig 6).

III. REFLECTION FROM METALLIZATION

In this section, we consider the effect of the sharp edges between waveguide and flange face (or between the groove and flange face) on the electrostatic insulation. It is clear that rounding these edges will spoil the choke principle, so we avoid it. Two solutions are possible: i) to accept the edges and their peaks of electric field ii) to cover the insulator faces with a thin metal layer, transparent to microwaves, but conducting static charges. Actually the metal layer may be replaced by semiconductors film, or anything else, with a given thickness d_C and conductivity σ .

As to microwave transmission, we can actually prove that solution ii) introduce no problems, at the nominal design value $\sigma d_c = 10^{-7}$ mho per square and within some order of magnitude from it. We expected that only the product σd_c matter; surprisingly enough, we see that result also depends weakly on σ alone. On the other side, using solution ii), the electrostatic field reduces to the parallel plate condenser one, which is the ideal case, while, in solution i), this field has some minor imperfection, shown by numerical computation, Clearly the latter solution is inferior on the basis of common witness in electrostatic, but to an extent which is difficult to precise (see later). Also microwave effect on electrostatic breakdown will be worth of some investigation.

III.A) *Microwave transmission through metallized windows in waveguides.*

In the computation of microwave transmission and reflection from metallization performed in this section, for the sake of simplicity we assume that the waveguide is continued also in the gap (previously considered as the DC-break), so that no power can leak: $L = 0$. This implies $\rho + A + \tau = 1$, where A is the absorption coefficient. In other words, we studied a DC-break without metallization in section II and now we study a metallized window without the DC-break.

Geometry is shown in Fig. 7 . Since x, y and z separates, there is no mode conversion of the incoming TE$_{10}$ mode, but only reflection at the interfaces; we label section 1 the incoming waveguide, 2 the first metal layer with real part of the relative dielectric constant ϵ_c and conductivity σ , 3 the dielectric foil of thickness d_d and complex relative dielectric constant $\epsilon = \epsilon_0 \epsilon_r (1 + i \tan \delta)$, 4 the second metal layer, identical to the first layer, and 5 the output waveguide. In the i-th section the field (similar to eq. (1)) may be expressed as as:

$$B_i^z = \frac{\pi E_0}{i\omega b} \cos(\pi x/b) \left(\alpha_i e^{ik_i z} + \beta_i e^{-ik_i z} \right) \tag{26}$$

where k_i is the wavenumber along z, depending on the medium, and α_i, β_i the dimensionless amplitude of the forward and backward wave; we note that $\alpha_1 = 1$ and $\beta_5 = 0$. It is

convenient to give a name to the z-factor of eq. (26) , as: $g_i(z) = E_0 \left(\alpha_i e^{ik_i z} + \beta_i e^{-ik_i z} \right)$. From eq. (1) also follows that:

$$E_y = \sin(\pi x/b) g(z) \qquad B_x = i\omega^{-1} \cos(\pi x/b) \partial_z g(z) \tag{27}$$

and $B_y = E_x = E_z = 0$. The wavenumbers are given by

$$k_1 = k_5 = \sqrt{\frac{\omega^2}{c^2} - \frac{\pi^2}{b^2}} \qquad k_3 = \sqrt{\epsilon_r \frac{\omega^2}{c^2} - \frac{\pi^2}{b^2} + i\omega\sigma_d\mu_0} \tag{28}$$

$$k_2 = k_4 = \sqrt{\epsilon_d \frac{\omega^2}{c^2} - \frac{\pi^2}{b^2} + i\omega\sigma\mu_0} \tag{29}$$

where $\sigma_d = \omega\epsilon_0\epsilon_r \tan\delta$ is the effective conductivity of the dielectric, which may be not negligible at our frequencies (for teflon $\delta = 0.0002$ and $\sigma_d = 3.4 \times 10^{-4}$ mho/m). We note that k_1 must be real and positive because we assume that the incoming wave propagates into the waveguide, k_3 has therefore a dominant real part which is positive and a small imaginary part which is positive, and only the square root of eq. (29) needs to defined by analytical continuation. When, as in normal cases, $\Im(k_i) \geq 0$ the α amplitudes refer to the forward wave and β to the backward wave; otherwise their roles will be interchanged.

Let z_i be the interface between section i and $i+1$. We put $d_1 = d_d/2$ and $d_2 = d_1 + d_c$ and choose the $z = 0$ origin in the middle plane of the dielectric foil; then we get $z_4 = -z_1 = d_2$ and $z_3 = -z_2 = d_1$.

From the interface conditions that B_z and $\partial_z B_z$ be continuous we find for each interface at $z = z_i$ ($i = 1, 2, 3, 4$) the following equation

$$\begin{aligned} \alpha_i e^{ik_i z_i} + \beta_i e^{-ik_i z_i} &= \alpha_{i+1} e^{ik_{i+1} z_i} + \beta_{i+1} e^{-ik_{i+1} z_i} \\ k_i(\alpha_i e^{ik_i z_i} - \beta_i e^{-ik_i z_i}) &= k_{i+1}(\alpha_{i+1} e^{ik_{i+1} z_i} - \beta_{i+1} e^{-ik_{i+1} z_i}) \end{aligned} \tag{30}$$

which can be written in matrix form:

$$M_i^l \begin{pmatrix} \alpha_i \\ \beta_i \end{pmatrix} = M_i^r \begin{pmatrix} \alpha_{i+1} \\ \beta_{i+1} \end{pmatrix} \tag{31}$$

where M_i^l and M_i^r are the matrices at the left and right-hand side of eq. (30) . We note that $\det M_i^l = 2k_i$ and $\det M_i^r = 2k_{i+1}$. Therefore we can invert M_i^l and after defining $M_i = (M_i^l)^{-1} \cdot M_i^r$, we find the matrix explicit form

$$M_i = \frac{1}{2k_i} \begin{pmatrix} (k_i + k_{i+1})e^{i(k_{i+1} - k_i)z_i} & -(k_{i+1} - k_i)e^{-i(k_{i+1} + k_i)z_i} \\ -(k_{i+1} - k_i)e^{i(k_{i+1} + k_i)z_i} & (k_{i+1} + k_i)e^{-i(k_{i+1} - k_i)z_i} \end{pmatrix} \quad ; \quad \det(M_i) = \frac{k_{i+1}}{k_i} \tag{32}$$

and the amplitude transformation at the interface:

$$\begin{pmatrix} \alpha_i \\ \beta_i \end{pmatrix} = M_i \begin{pmatrix} \alpha_{i+1} \\ \beta_{i+1} \end{pmatrix} \tag{31}$$

9

Combining the four interface condition, we find

$$
\begin{pmatrix} 1 \\ \beta_1 \end{pmatrix} = N \begin{pmatrix} \alpha_5 \\ 0 \end{pmatrix} \quad \text{with} \quad N = M_1 \cdot M_2 \cdot M_3 \cdot M_4 = \begin{pmatrix} n_{11} & n_{12} \\ n_{21} & n_{22} \end{pmatrix} \tag{33}
$$

where n_{ik} are the matrix element of N . We note that $\det N = k_5/k_1 = 1$. System (33)is trivially solved by

$$
\alpha_5 = 1/n_{11} \qquad \beta_1 = n_{21}/n_{11} \tag{34}
$$

Other amplitudes may be obtained by repeated application of eq. (31) from α_5 ; expressions are listed in appendix A.

The dissipated power in any given section or region is given by:

$$
D = \tfrac{1}{2} \int \mathrm{d}z \int_0^a \mathrm{d}y \int_0^b \mathrm{d}x \sigma |E_y|^2 \tag{35}
$$

where the electric field is related to eq. (26) from eq. (27) . It is convenient to perform the two integrations on x and y in eq. (35) , which gives $D = \tfrac{1}{4} ab \int \sigma |g|^2$. Since the incoming power is $P_{\mathrm{in}} = abE_0^2 k_1/(4\omega\mu_0)$ from eq. (4) , we can write the formula

$$
D = \frac{\omega\mu_0 P_{\mathrm{in}}}{k_1} \int dz \left| \alpha_i e^{ik_i z} + \beta_i e^{-ik_i z} \right|^2 = \frac{\sigma\omega P_{\mathrm{in}}}{k_1} \int dz |\alpha_i|^2 e^{-2k_i'' z} + |\beta_i|^2 e^{2k_i'' z} + 2\mathrm{Re}[\alpha_i \beta_i^* e^{2ik_i' z}] \tag{36}
$$

where the integration on z extends on the region(s) of interest, k_i is to be chosen accordingly and k_i' , k_i'' are its real and imaginary part. In particular, we can compute the total dissipated power D_c in the metal and the total dissipated power D_d in the dielectric; we define the adsorption coefficient $A_c = D_c/P_{\mathrm{in}}$ and $A_d = D_d/P_{\mathrm{in}}$. Their expression are also listed in appendix A.

III.B) *Conduction losses in treated teflon windows.*

Let us now discuss the wavenumber in the metal given by Eq. (29)in detail. We note two regimes, the poor conductivity one, given by

$$
\frac{\sigma}{\omega\epsilon_c} \ll 1 \tag{37}
$$

$$
\text{where} \quad k_2' \cong \omega\sqrt{\mu_0\epsilon_c} \qquad k_2'' \cong \frac{\sigma}{2}\sqrt{\frac{\mu_0}{\epsilon_c}} \tag{38}
$$

and the high conductivity one, where the expressions with physically corrected sign are:

$$
k_2' = \omega(\alpha\mu_0\epsilon_c)^{1/2} \left[\frac{1}{2}\sqrt{1 + \frac{\sigma^2}{\omega^2\epsilon_c^2\alpha^2}} + \frac{1}{2} \right]^{1/2} \qquad k_2'' = \omega(\alpha\mu_0\epsilon_c)^{1/2} \left[\frac{1}{2}\sqrt{1 + \frac{\sigma^2}{\omega^2\epsilon_c^2\alpha^2}} - \frac{1}{2} \right]^{1/2} \tag{39}
$$

Here the shorthand $\alpha = 1 - (\pi^2/\omega^2 b^2 \mu_0\epsilon_c)$ has values near to one. Note that the square bracketed factors, which are the only terms affected by σ , represent the wavelength compression due to the metal.

It can be noted that we allow the real part of the dielectric constant of the conducting film to be $\neq 1$, which is unusual. In our case, since the conducting film is made by ion implantation, we expected percolating carbon filaments, providing some conduction, dispersed into a matrix of still unburned polymer, which therefore still retain its $\epsilon \neq 1$. For practical estimates, we can then take $\epsilon_c = \epsilon'_d$. We note that σ actually changes with z, so that σ and d_c must be taken as fitted values (see graph in Fig. 7). Also note that while the product σd_c is measurable by static current readings, the separate factors are not.

We therefore plotted reflection, transmission and conduction losses A_c as a function of σd_c, considering realistic widths $d_c = 10^{-8} \div 10^{-4}$ m and two values of conductivity $\sigma = 1$ mho/m (Fig. 8) and $= 1000$ mho/m (Fig. 9). Comparing the two graphs, we saw that the coefficients for τ and D_c/P_{in} are clearly different for example at $\sigma d_c = 10^{-4}$ mho. The reason is that the imaginary part of k_2 from eq. (39) is not simply proportional to σ in those two graphs, as it was when $\sigma \ll 1.5$ mho/m.

For these reasons, we separately plot τ, ρ and $a = A_c/(\sigma d_c)$ for six decades of σ values ($10^{-3} \div 10^3$ mho/m) in Figs. 10, 11 and 12 respectively.

A remarkable flat plateau appears in Fig. 12, where $a = 890 \pm 15$ ohm. Since $A_c < 1$ by energy conservation, a is bounded by $1/(\sigma d_c)$, that explains the steep slope at $\sigma d_c > 0.01$ mho, which limits the plateau on one side. A rough explanations for the a plateau is the following. When the metal thickness d_c is much smaller than the penetration depth, the reflections on the two surfaces are of about equal strength and cancel each other in the backward direction (provided that d_c is much smaller than the wavelength λ, which is usually true); moreover absorption is negligible, so that transmitted wave approximates the incoming one. In particular the ratio $Z = -E_y/H_x$, known as wave impedance, remains about its value for incoming and transmitted waves, which is $Z_w = \mu_0 \omega/k_1 = 501$ ohm. Similarly, when the dielectric sheet is much thinner than half wavelength, the reflections from the two faces almost cancel, and the ratio Z can not deviate very much from Z_w. Consistently, the power flow $P(z) = \frac{1}{2} \int \mathrm{d}x \mathrm{d}y E_y H_x^*$ (compare with eq. (4), the half factor is due to complex representation) is conserved and is about equal to P_{in} at any z.

Substituting $H_x \cong -Z_w E_y$ in $P(z)$ expression, we find $\int \mathrm{d}x \mathrm{d}y |E_y^2| \cong 2P_{\text{in}} Z_w$, so that eq. (35) simplifies to

$$D_c = \int_{\text{regions } 2,4} \mathrm{d}z \sigma P_{\text{in}} Z_w = 2Z_w P_{\text{in}} \sigma d_c \tag{40}$$

showing that $a \cong 2Z_w = 1000$ ohm, in good agreement with plateau value.

When d_c is comparable to λ, the above argument no longer holds, and few valley and crests appear in fig. 12; the first valley corresponds to $d_c = 3.8 \pm 0.17$ mm, or $d_c/\lambda = 0.18$.

From Fig. 12, we note that $D_c/P_{\text{in}} < 10^{-4}$ for every σ at the nominal $\sigma d_c = 10^{-7}$ mho per square. This is smaller than the dielectric loss $0.000180 P_{\text{in}}$, so that the thermal stability of treated window is about the same as the one of simple windows. It is interesting to note that losses in the flanges themselves are greater, (in the order of $10^{-3} P_{\text{in}}$) and that the nearby waveguides also produce some heating.

For these reasons and according to the past experience with a DC-break, where heating was noticeable at 400 W forward power level when water cooling was off, we decided to keep a limited cooling in the choke flange.

III.C) *Electrostatic field*

In the comparison for the insulation of a metallized and a simple dielectric sheet we consider the electric field component E_z and $E_{\text{para}} = \sqrt{E_x^2 + E_y^2}$ on both sides of the sheet

(the one facing choke is $z = 0$, the other is at $z = d$; we held the choke flange at the potential $V = 0$ and the other flange at $V = V_s$). For a metallized sheet we have

$$E_x = E_y = E_{\text{para}} = 0 \qquad E_z = V_s/d = 2\ 10^5 \ \text{V/cm} \qquad (41)$$

where in numerical examples we set $V_s = 20$ kV and $d = 1$ mm. For a simple window, the geometry imposes numerical solution (with TOSCA [10]) of the flanges; in Fig. 13 the fields at $y = z = 0$ as a function of x are shown.

Since E_{para} is parallel to the air-teflon interface, it may produce local discharge much before the E_z component perforates the sheet; anyway this local discharge is likely to be self-estinguished when no microwave are present, because it creates either a permanent surface charge or a transient surface plasma near the window sides, which shorts the electrostatic field as well as the metallization will do. The charge surface density at which this happens is $\sigma_c = V_s \epsilon_0 = 0.177 \ \mu\text{C m}^{-2}$ so that the total charge in the groove C_g and in the waveguides C_{in} , C_{out} are:

$$C_g = 2\pi w_g R_g \sigma_c = 29 \ \text{pC} \qquad C_{\text{in}} = C_{\text{out}} = ab\sigma_c = 22 \ \text{pC} \qquad (42)$$

When there are microwaves, both the the transient discharge and the surface charge/plasma may initiate a waveguide arc; whether this actually happens notwithstanding the small charges involved is of course a subject of future experimental investigation.

A point that can hardly be doubted is that E_x is enough to trigger a local discharge: we have $E_x = 1.4 \ 10^5$ V/cm at waveguide "in " edge and $E_x = 2 \ 10^5$ V/cm at the groove edge. In Fig. 13 we show the potential as well, to give an idea of the voltage drop V_d available to local discharges, which results to be $V_d \cong V_s/2 = 10$ kV; this value confirms the possibility of discharges.

Therefore we have to imagine that a cloud of electrons stays on the teflon whenever the voltage V_s is on. Two testable conclusions seems to follow: 1) turning microwave on first and the voltage later, is by far more dangerous than the time reversed procedure; 2) if the source voltage falls significantly, as a result of a spark elsewhere but the DC-break, this electronic cloud disperses and flows to the waveguide walls; this transient discharge may also originate a waveguide arc. The conclusion 2) shows that correlation between sparks and waveguide arcs is not unexpected, and it is not a conclusive evidence for blaming the DC-break as the sparks origin.

As regards to E_z of Fig. 13 , we note that its value in the waveguide is generally less then eq. (41) because effective gap width is there a and not d ; anyway, E_z rises to 20-30% above the eq. (41) value at groove and waveguide edges. These peaks are a further drawback of a simple window. Anyway, the destructive event of a dielectric perforation (1) may be excluded because the field disuniformity is not great and the total voltage drop is constrained to be V_s , either for the uniform field of a metallized window or the nonuniform field of a simple window and consistently (2) it was never observed on the old DC-break teflon sheets.

For sake of completeness, we show the electric fields on three other lines, finding lower absolute values, but similar behaviour to Fig. 13 . In Fig. 14 , we move on the flat flange side of the teflon, so that the E_x peak disappears at the groove. In Fig. 15 , we follow the diagonal of the rectangular guide, therefore encountering a corner, which has a shielding effect; the field E_x, Ey are thus smaller than before, and moreover, E_y is about double of E_x . Afterwards, we encounter the groove, where the fields are nearly equal to the previous case. In Fig. 16 we follow the diagonal, but staying on the flat flange teflon side. Corner fields are similar as before. The groove related peaks of E_x, E_y of course disappear; still we have a valley in E_z .

12

IV. THE ANTENNA

Even if the E-H tuners in microwave circuit of Fig. 1 may compensate for reflection of the load (the plasma plus the antenna) up to a VSWR (Voltage Standing Wave Ratio) of five or ten, we consider an antenna design satisfactory when the VSWR is less than 2, for any plasma condition; this corresponds to a reflection coefficient less than 13 % of the incoming power and to a maximum microwave field $E_y^M = (1 + \sqrt{\rho})E_0 \cong 1.4E_0$.

This restriction is motivated by reducing the risks of waveguide arcs and the complexity of the tuning operation. An effective tuning is anyway always possible: the frequency f of the klystron has a maximum bandwidth of 80 MHz, by construction. Once tuned, the bandwidth of the tuned circuit is about

$$B \cong \tfrac{1}{2}f\lambda_g/(2L_t) = 120 \quad \text{MHz} \tag{43}$$

where L_t is the distance of tuners from the plasma ($L_t = 80 - 100$ cm).

It may be argued that the presence of the plasma may affect the operation of the antenna, so that antenna geometry and plasma effects must be considered together; in principle, a coupling scheme such that the antenna reflection cancels the plasma reflection is acceptable (and is used in high plasma density ECR dedicated to one plasma production, such as in film deposition [12]).

One reason for separate studies and zeroing of antenna and plasma reflections is that the latter will change, according to the plasma density; in highly charged ion ECR, density ranges from tenuous to moderately dense plasma depending of current required. The second reason is that plasma reflection may be negligible in most of the mentioned regimes and antenna reflection zeroing can be studied as it radiates in air. Note that we can easily measure the reflection with plasma on and off and thus check the two zeros.

The third reason, specific to the Alice source, is that, experimentally, the reflection from the first stage ρ_1 is zero (within 1 %), while the second stage reflection ρ_2 is 40 % ; both values do not significantly change when plasma is turned on or off. This is consistent with the conjecture that Alice plasma is tenuous, based on low value of the extracted current (limited to 350 μA). We exclude that second stage circuit may be wrongly mounted by accidents. Understanding in physical and simple terms why the second stage antenna exhibits this defect is therefore of great importance.

In the Alice source, the antenna may suffer from the nearby camera walls (see Fig. 17), which are in the near field region. To simply compare the old coupler of Alice, two ideal directivity couplers and two partial directivity couplers we will use geometric optics arguments.

Let x' be the major and y' the minor sides of the guide cross-section. We can decompose the incoming TE$_{10}$ wave of eq. (27) into two plane waves:

$$E_y = \exp(ik_x x' + ik_z z) \tag{44}$$

where $k_x = \pm\pi/b$ and $k_z = k_g$ inside the antenna. When these waves leave the guide aperture, they are diffracted; tracing the two rays with direction $\vec{k} = (k_x, 0, k_g)$ at start provides an approximate map of the surfaces more directly illuminated by the incoming radiation; let P_1 be the center of the antenna aperture and Q_1 the wall point where the ray from P_1 impinges (see Fig. 17). These rays make an angle $\theta_g \cong 41^0$ with the z-axis, while the intensity of far field of the antenna falls below half maximum for $\theta > 60^0$; from which the outer diffraction angle is $\alpha = 19^0$. An estimate of error δ_s on the size s of illuminated

13

region is the diffraction angle in $x'z$ plane times the distance $\overline{P_1Q_1} = \frac{1}{2}b\sec\theta_g$; that is $\delta s = (\frac{1}{2}b\tan\alpha)\sec\theta_g = 0.4$ cm.

Consider first the previous coupler A of the second stage, obtained by rotating the guide cut plane from $x'y'$ by an angle $\psi = 60^0$ around the x' axis (see Fig 18); note that the guide aperture watches directly the nearby Alice walls, located just below. This circumstance clearly favours producing reflected waves, since rays bouncing on Alice walls are upwards reflected and graze the waveguide tip, as seen in Fig. 17 . Anyway, quantitative determination of backscattered radiation, due to diffraction effects, requires further investigation and can not be represented by ray tracing. Indeed, since the rays will reflect on surfaces which are independent on z (the normal $\mathbf{n}$ has no z-component) the quantity k_z will remain constant (only the $\mathbf{k}$ component which is parallel to $\mathbf{n}$ may change). Therefore k_z remain positive, that is, rays go forward.

With the reverse cut $\psi = -60^0$ (coupler B, used in the first stage of Alice), the tip will be located under ray paths, thus intercepting none. We conclude that ray tracing can at least signals whether a design is risky or not.

Note that analytic approach must use the full integrals of the Stratton-Chu formula as

$$\int_S l(P)\frac{\exp[i\omega(d(P,Q)-ct)/c]}{d(P,Q)}\mathrm{d}S \tag{45}$$

where S is the guide aperture, P a point spanning it, and Q a point on the wall; d is their distance; Fraunhofer or Fresnel approximations are excluded because $d(P,Q) \cong b \cong \lambda$. Computational evaluation of the coupler is in principle straightforward but: i) requires a 3D-code, commercial or ad hoc written; ii) requires a preliminary selection of candidate design.

It is well-known that an ideal directivity coupler C can be simply achieved by rotating the cut plane from $x'y'$ by an angle $\theta = \text{arctg}(k_g/k_b) = 49.1^0$ around the y' axis, so to be parallel to one wave direction $(-k_b, 0, k_g)$; the full power is then emitted in the other wave $\vec{k} = (k_b, 0, k_g)$.

We note that this coupler therefore avoids illuminating walls within 5 cm; this distance is enough to attenuate reflection back to the antenna. Unfortunately this coupler will take 18 mm of ECR cavity, with serious plasma perturbations. We therefore consider a partial directivity coupler D obtained with $\theta \cong 20^0 - 30^0$ (6 − 9 mm long).

Other possibilities include a reversed ideal directivity coupler E with $\theta = -49.1^0$ or coupler F consisting in a simple guide cut: $\theta = \psi = 0$.

For comparison, the usual impedance analysis can be applied to coupler F (let us neglect the nearby wall). Since the wave impedance is $Z_w = \omega\mu_0/k_z = 501$ ohm in the waveguide and abruptly changes to the vacuum impedance $Z_v = 377$ ohm, an estimate for the reflection coefficient is

$$\rho_F \cong \left|\frac{Z_v - Z_w}{Z_v + Z_w}\right|^2 = 0.0200 \tag{46}$$

In summary, eventual numerical simulations will mainly have to clarify the effect of nearby walls; two continuous parameters (the position of antenna middle $z(P_1)$ and the cut angle, θ or ψ depending on coupler model) must be explored.

14

V. PLASMA ADSORPTION AND CAVITY MODEL

The interaction of microwaves with ECR plasma has been subject of renewed interest [13]. In the linearized theory of homogenous plasma, we find different waves depending on the angle α between the ion source magnetic field $\mathbf{B_0}$ and the wavenumber $\mathbf{k}$. Note that $\mathbf{B_0}$ is a stationary field, while $\mathbf{E}$ and $\mathbf{B}$ refers to the pure microwave field, as in the previous chapter.

To clearly understand the limits of our results, it is worthwhile to first specify the process, necessarily oversimplified, which represents microwave absorption in our analysis, namely an effective friction acting on electrons: the Krook model [14]. In steady state plasmas, microwave absorption is actually due to the electron being first accelerated, and afterwards, losing their energy again (in ionization reactions or wall impact). We discuss here the simplest approximation in which electrons suffer a simple friction only: $\vec{F} = -m_e \nu \vec{v}_e$ where ν is an effective collisional frequency independent from electron velocity (as it actually happens when collisions against neutrals are dominant), so that electron cyclotron oscillation therefore stabilizes at a stationary speed and radius [14]:

$$x_1 = -\frac{w e E_1}{\omega m_e (w^2 - \Omega^2)} \qquad x_2 = i\frac{\Omega}{w} x_1 \quad x_3 = -\frac{e}{\omega w} E_3$$

$$\vec{v}_e = -i\omega \vec{r}_e \tag{47}$$

Here the shorthand $w = \omega + i\nu$, widely used in the following, is introduced; $x_1 x_2 x_3$ is a locally orthogonal coordinate system whose x_3 axis is taken parallel to the external magnetic field B_0; also $E_2 = 0$ may be assumed without any loss of generality. This model is strictly valid only when ν is greater than the bouncing frequency of electrons in ECR mirrors and ν is high enough to maintain the electrons non relativistic and to maintain the phase of the electron oscillation random with respect to microwave. When this model breaks down, the absorbtion may saturate for relativistic effects, or depletion of phase space distribution of electrons and/or wrong phase between electron oscillation and microwave (electron bunching, known also as superadiabaticity). Moreover electrons may actually transport energy through the plasma.

In our model of the ECR plasma, we may safely assume that plasma density is stationary, respect to microwave period (the converse would imply relativistic plasmoids); a fortiori, the external magnetic field B_0 is stationary. Therefore, modes with a definite ω are possible. With the parameter of the ECR Alice [2], the wavelength $\lambda = 2\pi c/\omega = 2.08$ cm is in the order of spatial plasma dimension, so that k is not precisely defined. Anyway, the gyroradius of electrons is $r_{el} = \lambda\beta/2\pi$; for cold or warm electrons $\beta \leq 0.1$ the adiabatic motion therefore still holds, so that the permittivity tensor $K_{il} = 1_{il} - (i\omega\epsilon_0)^{-1}(\delta j_i/\delta E_l)$ is expressed as:

$$K = \begin{pmatrix} K_1' & K_2' & 0 \\ -K_2' & K_1' & 0 \\ 0 & 0 & K_3' \end{pmatrix} \tag{48}$$

where in terms of the plasma frequency ω_{pl} and the cyclotron frequency Ω , the elements are

$$K_1' = 1 - \frac{\omega_{\mathrm{pl}}^2 w}{\omega(w^2 - \Omega^2)} \tag{49}$$

15

$$K_2' = -i\frac{\Omega\omega_{\mathrm{pl}}^2}{\omega(w^2 - \Omega^2)} \tag{50}$$

$$K_3' = 1 - \frac{\omega_{\mathrm{pl}}^2}{\omega w} \tag{51}$$

From the Maxwell equation $\mathrm{rot}\,\mathbf{B} = \mu_0(\mathbf{j} + \epsilon_0\partial_t\mathbf{E}) = -i\omega\mu_0\epsilon_0 K \cdot \mathbf{E}$, we get the vectorial mode equation:

$$\frac{c^2}{\omega^2}\,\mathrm{rot}\,\mathrm{rot}\,\mathbf{E} = K \cdot \mathbf{E} \tag{52}$$

It will be convenient to scale the matrix element according to $K_1 = K_1'\omega^2/c^2$, so that eq. (52) simplifies.

Generally speaking, the tensor K depends on r, ϑ, z both through the scalar quantities ω_{pl} , $|\Omega|$ (and eventually ν if desired) and because its principal axis 3 must rotate to follow the $\mathbf{B}_0$ direction.

V.A) *The solvable model.*

We can reduce to a solvable model by assuming that: 1) the component B_z is much greater than the other, so that our principal axes 1,2,3 are approximately xyz ; 2) plasma density and magnetic field intensity depend only on z . In particular K_1 K_2 and K_3 are functions of z, not of x or y .

We introduce the scalar quantity $W = \partial_x E_y - \partial_x E_x$, which is proportional to the wave $B_z = Wc/\omega$ according to Faraday law; therefore W is proportional to the usual potential of TE modes. By applying $-\partial_y$ and ∂_x to the first and second component of (52) respectively, and summing, we get

$$(K_1 + \triangle)W = K_2 T \tag{53}$$

with $T = \partial_x E_x + \partial_y E_y$. This equation is not closed for the presence of Z , due to the external magnetic field B_0 through coefficient K_2 .

We note that a longitudinal wave can also be present, but provided that $K_3 \neq 0$ everywhere, that is the low density regime:

$$\omega_{\mathrm{pl}} \ll \omega \tag{54}$$

this wave will not be excited resonantly by W .

An approximate argument may simply relate T to W ; consider the sum of ∂_x applied to first of eqs. (52) and ∂_y applied to the second one:

$$-\partial_z^2 T = K_1 T + K_2 W + O(E_z) \tag{55}$$

By assuming a decomposition in right- and left-handed polarized waves

$$T_s = isW_s \quad \text{with} \quad s = \pm 1 \tag{56}$$

and neglecting terms of order $\triangle_\perp = \partial_x^2 + \partial_y^2$, both (53) and (55) simultaneous reduce to the same equation

$$W_s''(z) + (K_1 + isK_2 + \triangle_\perp)W_s = 0 \tag{57}$$

The ECR cavity is a steel or copper cylinder; surface resistance will be neglected. With minimal idealization, we imagine the cylinder connected to the guide at the surface A1,

cut into the first base. Let BC1 be the first base at $z = 0$ except for the antenna cut A1, CB2 the second base at $z = L$ where the beam extraction hole is located (this hole will be neglected) and BC3 be the lateral boundary at $r = D/2$.

Consistently with eq. (56) , the lateral boundary conditions are $\partial_r W \cong 0$ and $\partial_r T = 0$ at $r = D/2$ (BC3).

On BC1 and BC2,

$$B_z = 0 \qquad E_x = 0 \qquad E_y = 0 \tag{58}$$

since these conditions hold on $z = \text{const.}$ planes, they can be differentiated on x and y to give

$$W = 0 \qquad\qquad T = 0 \tag{59}$$

that is consistent with decomposition (56) .

On the antenna surface A1, the field should match with the incoming and reflected TE$_{10}$ mode when we neglect the evanescent mode in the guide for the sake of simplicity; so we find:

$$W(x', y', z) = A(x', y')(e^{ik_z z} + \alpha e^{-ik_z z}) + \quad \text{ev. modes}$$

$$\partial_z W(x', y', z) = ik_z A(x', y')(e^{ik_z z} - \alpha e^{-ik_z z}) + \quad \text{ev. modes} \tag{60}$$

at $z = 0$, where k_z is a real number, x' y' are translated axes to coincide with the waveguide sides and A is the antenna pattern

$$A(x', y') = E_0 k_b \cos(k_b x) \tag{61}$$

from the TE$_{10}$ fields of eq. (1) .

We can separate eq. (57) in cylindrical coordinates

$$W_s(x, y, z) = \sum_{ms} W_m(z) Y_{ms}(x, y) \quad \text{where} \quad \triangle_\perp Y_m = \gamma_m Y_m \tag{62}$$

with Y_m satisfying the boundary condition at BC3; here m is a couple of integer indexes (there is no convenience to write m_1, m_2 in detail). Note that $\gamma_m < 0$. The eq. (63) becomes now :

$$V(z) W_{ms}(z) + \partial_z{}^2 W_{ms}(z) = 0 \quad \text{where} \quad V(z) = K_1^2 + is K_2 + \gamma_m \tag{64}$$

is the effective (complex) potential. From eqs. (60) and (62) we see that the antenna excites (mainly) modes with $-k_b^2 \leq \gamma_m < -(1.854/D)^2$ (the upper bound is not zero, because of finite Alice radius). By standard mode decomposition of (60) , and matching, we see

$$\frac{1 - \alpha}{1 + \alpha} = Z_{\text{ECR}} = \sum Z_{ms} g_m \quad \text{where the "mode impedances" are} \quad Z_{ms} = \frac{W'_{ms}(0)}{ik_z W_{ms}(0)} \tag{65}$$

and their weights are $g_m = |(Y_m, A)|/2(Y_m, Y_m)$ with the usual scalar product in function spaces $(,)$. The reflection is $\rho = |\alpha|^2$ and Z_{ECR} is so recognized as the dimensionless impedance of the whole source.

V.B) *Parameters and quantities of interest to numerical simulations.*

We must study numerically eq. (64) for several values of γ_m, in particular

$$\gamma_M = -2 \ \text{cm}^{-2}$$

17

and $\gamma_m = -0.1, -3.9$ cm^{-2} .

Even if a weighted average of Z over several γ_m and the two signs of s is the detectable quantity according to eq. (65) , note that table I,II separately report the results for particular γ_m values because: i) they are more easily computed; ii) they depend only on the ECR cavity and not on the antenna; iii) they show trends, due to varying magnetic field or attenuation parameters, clearly; iv) the case $\gamma_m = \gamma_M$ is about the average for the $s = +1$ band.

It is interesting to compare the cases $k_z = k_g = \sqrt{(\omega/c)^2 - (\pi/b)^2}$ (waves launched by a rectangular waveguide) and $k_z \cong \omega/c$ (coaxial microwave injection). In table I (respectively table II) we indeed summarize results for the mode dimensionless impedance $Z_{m,+}$ (respectively $Z_{m,-}$), the reflection coefficient ρ_w for coupling a wave coming from the standard WR62 waveguide in a ECR cavity given mode m, s , and the reflection coefficient ρ_v for coupling an incoming plane wave $k_z = \omega/c$; they are computed from

$$\rho_v = |\alpha_v|^2 \quad \text{with} \quad \frac{1 - \alpha_v}{1 + \alpha_v} = \frac{W_{ms}(0)}{ik_z W_{ms}} = Z_{ms}\frac{k_g}{k_z} \tag{66}$$

and a similar equation for ρ_w .

To observe the reflections listed in tables I,II, we should prepare a incoming wave with a given γ_m and s . Practically, the circular polarization sign can be set easily, provided a circular waveguide is used; this is an idea for future experiments (some ECR actually use circular waveguides, so this is easy to try; Alice use rectangular guides, so that a new Removable Plasma Chamber with proper guides must be built, that is not feasible now). Selecting γ_m seems practically impossible (a phased array of antenna, as large as the plasma chamber itself, should be used; this plugs the pumping manifolds, etc.).

The effects of changing ν also are of the outmost importance and were partly studied. In numerical simulations we set the cavity length at $L = 18$ cm and the microwave frequency at 14.4 GHz, corresponding to a $\omega/c = 3.04$ cm^{-1} ; we found convenient to use quantities with dimension of a power of length, for comparing all physical effects together, and to restrict to Alice values for those parameters. Plasma density may be assigned as a function of z in our model , but we take it as a constant; we set $\omega_{\text{pl}}/\omega = 0.4$ which is believed to be a transition value from tenuous to moderately dense plasma [13] or $\omega_{\text{pl}}/\omega = 0.7$ representing a moderately dense plasma. Note that from our model a ponderomotive pressure on microwave on plasma may de inferred, so that profile of $\omega_{\text{pl}}(z)$ can be computed in a next model, provided that we oversimplify all plasma transport and confinement processes (by taking a perfect gas equation for instance).

We also study the effect of changing the magnetic field; in detail, assuming a parabolic dependence:

$$B_z = \frac{m_e c^2}{e} \left(\frac{b_l + (b_m - b_l)(2z - L)^2}{L^2} \right) \tag{67}$$

where the parameters must satisfy $b_l < \omega/c < b_m$ in order to obtain ECR resonance somewhere. We indeed changed the parameter b_l from 0 to 2.5 cm^{-1} and b_m from 3.5 cm^{-1} to 6.5 cm^{-1} .

Numerical integration method needs further improvements. In table I we also give the fixed step length Δz used in the Runge-Kutta integration of eq. (64) . An adaptive Runge-Kutta is under development. We try to adapt the step in order to maintain the relative change of the adiabatic constant:

$$I = \frac{|W(z)|^2 + |V(z)||W'(z)|^2}{2|V(z)|^{1/2}} \tag{68}$$

18

lower than a given ϵ_K. This criterion is probably too severe, and leads to prohibitive long calculation when ν/ω is less than 0.05 and/or ϵ_K less than 10^{-3} .

V.C) *Results for mode impedances and reflections.*

In Fig. 19 we show results for $\omega_{pl}/\omega = 0.7$, $b_l = 2.$ cm^{-1}, $b_m = 5$ cm^{-1}, $\gamma = \gamma_M$ as a function of ν/ω . For $\nu/\omega > 0.0001$ absorption is constant and dominant (0.94 for waveguide, 0.99 for plane wave). The small reflection of the waveguide case is related with waveguide to ECR cavity mode matching, and it is not due to plasma reflection. Indeed the properly launched plane wave is completely absorbed.

For $10^{-6} \leq \nu/\omega \leq 10^{-4}$ we find a considerable reflection, but a surprisingly high absorption, related to peaks in the imaginary part of V and concentrated in a small region of space. In this region, numerical errors are not completely under control. By an accident with $\Delta z = 0.001$, both ρ_v and ρ_w may be well fit to the formula

$$\rho = A + B \exp(-\nu/\nu^c) \tag{69}$$

where $A_v = 0.0106$ $B_v = 0.987$ and $\nu_v^c = 6.77 \times 10^{-6}$ for the air launched wave. Similarly, $A_w = 0.055$ $B_w = 0.95$ and $\nu_w^c = 7.3 \times 10^{-6}$ for the guide launched wave.

Note that the fit formula is consistent with ρ_v or $\rho_w = 1$ at $\nu = 0$. For $\nu = 0$ we indeed must have total reflection, since W_m is then real and therefore Z_M is imaginary, so that $|\alpha| = 1$ from Eqs. (65) or (66) . Physically this means that there is no absorption process.

In Fig. 20 a profile of W_+ is shown for a typical case. Note that W amplitude is constant up to the first resonance, where it dies out, as it would be for a plane wave encountering a perfect absorber. No electric field adiabatic compression happens, since a 2 cm wavelength is not adiabatically small respect to the width of the $V(z)$ peak. This simple consideration has obvious implication on the electron acceleration mechanism in ECR plasma, clearly favouring multistep bouncing acceleration.

To study b_m and b_l changes we take a comfortably high $\nu/\omega = 0.2$, so that Runge-Kutta become completely reliable (because V is smooth). We note that reflections are uniformly increasing when b_m is decreased down to 3.5 cm^{-1}, which is a lowest value acceptable for ECR operation (at 14.4 GHz). This confirms the opportunity to inject microwaves from high field side of the mirror.

No dramatic effects of changing b_l are evident.

APPENDIX A

From eq. (32) we find convenient to define the wavenumber combinations

$$q_{i+} = k_i + k_{i+1} \qquad q_{i-} = k_i - k_{i+1} \qquad O_i = \frac{1}{2k_i} \begin{pmatrix} q_{i+} & q_{i-} \\ q_{i-} & q_{i+} \end{pmatrix} \tag{A.1}$$

and the matrix valued function

$$D(\alpha) = \begin{pmatrix} e^{i\alpha} & 0 \\ 0 & e^{-i\alpha} \end{pmatrix} \tag{A.2}$$

With these notations we find:

$$M_i = D(-k_i z_i) O_i D(k_{i+1} z_i)$$

19

Table I : Results for right-handed polarized waves.

δz	γ_m	ν/ω	ω_{pl}/ω	b_l	b_m	$\Re[Z_{m,+}]$	$\Im[Z_{m,+}]$	ρ_v	ρ_w
cm	cm^{-2}	—	—	cm^{-1}	cm^{-1}	—	—	—	—
0.002	-0.10	1.0	0.4	2.0	5.0	1.369833	7.2051182E-02	9.3780499E-04	2.5255308E-02
0.002	-0.10	0.4472136	0.4	2.0	5.0	1.425920	7.2108373E-02	1.9142802E-03	3.1680569E-02
0.002	-0.10	0.20	0.4	2.0	5.0	1.460219	4.6464425E-02	2.4805556E-03	3.533706E-02
0.002	-0.10	8.9442715E-02	0.4	2.0	5.0	1.471102	2.6302898E-02	2.6532477E-03	3.6454469E-02
0.002	-0.10	0.04	0.4	2.0	5.0	1.474013	1.5976170E-02	2.6984930E-03	3.6749505E-02
0.002	-0.10	1.0	0.7	2.0	5.0	1.472406	0.2035688	7.8482255E-03	4.2996056E-02
0.002	-0.30	1.0	0.7	2.0	5.0	1.459372	0.2053839	7.5600543E-03	4.1572478E-02
0.002	-0.50	1.0	0.7	2.0	5.0	1.446227	0.2072505	7.3108682E-03	4.016466E-02
0.002	-0.70	1.0	0.7	2.0	5.0	1.432963	0.2091659	7.102617E-03	3.8773268E-02
0.002	-0.90	1.0	0.7	2.0	5.0	1.419595	0.2111347	6.9383057E-03	3.7402436E-02
0.002	-1.1	1.0	0.7	2.0	5.0	1.406106	0.2131666	6.8206894E-03	3.6053125E-02
0.002	-1.3	1.0	0.7	2.0	5.0	1.392492	0.2152478	6.7516607E-03	3.4726068E-02
0.002	-1.5	1.0	0.7	2.0	5.0	1.378752	0.2173931	6.7349919E-03	3.3424865E-02
0.002	-1.7	1.0	0.7	2.0	5.0	1.364892	0.2196049	6.7739524E-03	3.215289E-02
0.002	-1.9	1.0	0.7	2.0	5.0	1.350900	0.2218809	6.8716160E-03	3.0911570E-02
0.002	-2.1	1.0	0.7	2.0	5.0	1.336778	0.2242310	7.0320452E-03	2.9705083E-02
0.002	-2.3	1.0	0.7	2.0	5.0	1.322515	0.2266557	7.2590788E-03	2.8535530E-02
0.002	-2.5	1.0	0.7	2.0	5.0	1.308110	0.2291546	7.5567006E-03	2.7406499E-02
0.002	-2.7	1.0	0.7	2.0	5.0	1.293571	0.2317346	7.9295170E-03	2.6322959E-02
0.002	-2.9	1.0	0.7	2.0	5.0	1.278876	0.2344058	8.3830236E-03	2.5288172E-02
0.002	-3.1	1.0	0.7	2.0	5.0	1.264036	0.2371685	8.9219613E-03	2.4307450E-02
0.002	-3.3	1.0	0.7	2.0	5.0	1.249036	0.2400260	9.5521249E-03	2.3384834E-02
0.002	-3.5	1.0	0.7	2.0	5.0	1.233882	0.2429862	1.027951E-02	2.2526663E-02
0.002	-3.7	1.0	0.7	2.0	5.0	1.218567	0.2460596	1.1111109E-02	2.1739064E-02
0.002	-3.9	1.0	0.7	2.0	5.0	1.203080	0.2492429	1.2053504E-02	2.1027315E-02
0.002	-0.10	0.20	0.7	2.0	5.0	1.714775	0.1196028	1.7555159E-02	7.1124882E-02
0.002	-0.30	0.20	0.7	2.0	5.0	1.703435	0.1204895	1.6774010E-02	6.9552489E-02
0.002	-0.50	0.20	0.7	2.0	5.0	1.692028	0.1213873	1.6004696E-02	6.7977846E-02
0.002	-0.70	0.20	0.7	2.0	5.0	1.680541	0.1223094	1.5247332E-02	6.6399828E-02
0.002	-0.90	0.20	0.7	2.0	5.0	1.668987	0.1232564	1.4503667E-02	6.4820878E-02
0.002	-1.1	0.20	0.7	2.0	5.0	1.657344	0.1242176	1.3772830E-02	6.323821E-02
0.002	-1.3	0.20	0.7	2.0	5.0	1.645618	0.1252114	1.3056647E-02	6.1653852E-02
0.002	-1.5	0.20	0.7	2.0	5.0	1.633824	0.1262190	1.2356513E-02	6.0069989E-02
0.002	-1.7	0.20	0.7	2.0	5.0	1.621930	0.1272506	1.1671616E-02	5.8482956E-02
0.002	-1.9	0.20	0.7	2.0	5.0	1.609961	0.1283102	1.1004797E-02	5.6897383E-02
0.002	-2.1	0.20	0.7	2.0	5.0	1.597892	0.1293903	1.0355374E-02	5.5310160E-02
0.002	-2.3	0.20	0.7	2.0	5.0	1.585735	0.1305020	9.7255837E-03	5.3724162E-02
0.002	-2.5	0.20	0.7	2.0	5.0	1.573498	0.1316418	9.1170026E-03	5.2141327E-02
0.002	-2.7	0.20	0.7	2.0	5.0	1.561158	0.1328065	8.5294954E-03	5.0559089E-02
0.002	-2.9	0.20	0.7	2.0	5.0	1.548728	0.1340031	7.9654558E-03	4.8980795E-02
0.002	-3.1	0.20	0.7	2.0	5.0	1.536204	0.1352334	7.4260756E-03	4.7406748E-02
0.002	-3.3	0.20	0.7	2.0	5.0	1.523565	0.1364944	6.9119078E-03	4.5835409E-02
0.002	-3.5	0.20	0.7	2.0	5.0	1.510839	0.1377923	6.4259339E-03	4.4271704E-02
0.002	-3.7	0.20	0.7	2.0	5.0	1.497997	0.1391208	5.9685013E-03	4.2713050E-02

Table I continues.

δz	γ_m	ν/ω	$\omega_{\mathrm{pl}}/\omega$	b_l	b_m	$\Re[Z_{m,+}]$	$\Im[Z_{m,+}]$	ρ_v	ρ_w
cm	cm^{-2}	—	—	cm^{-1}	cm^{-1}	—	—	—	—
0.002	-3.9	0.20	0.7	2.0	5.0	1.485063	0.1404946	5.5428082E-03	4.1164387E-02
0.002	-2.0	0.20	0.7	2.0	6.5	1.448848	5.3694744E-02	2.2254782E-03	3.4059357E-02
0.002	-2.0	0.20	0.7	2.0	5.5	1.536609	9.1334306E-02	6.2436024E-03	4.5988426E-02
0.002	-2.0	0.20	0.7	2.0	4.5	1.698011	0.1972336	1.9001050E-02	7.1892440E-02
0.20	-2.0	0.20	0.7	2.0	3.5	1.950977	0.6812741	7.5788185E-02	0.1491967
0.20	-2.0	0.20	0.7	0.0	5.0	1.598025	0.1377000	1.0618538E-02	5.5637844E-02
0.002	-2.0	0.20	0.7	2.0	3.5	1.950181	0.6800904	7.5602449E-02	0.1489584
0.002	-2.0	0.20	0.7	0.0	5.0	1.597776	0.1379805	1.0613670E-02	5.5615246E-02
0.002	-2.0	0.20	0.7	0.50	5.0	1.599364	0.1357576	1.0631623E-02	5.5743217E-02
0.002	-2.0	0.20	0.7	1.0	5.0	1.600928	0.1334976	1.0648793E-02	5.5868395E-02
0.002	-2.0	0.20	0.7	1.5	5.0	1.602448	0.1311926	1.0663876E-02	5.5987902E-02
0.002	-2.0	0.20	0.7	2.0	5.0	1.603931	0.1288487	1.0677409E-02	5.6102894E-02
0.002	-2.0	0.20	0.7	2.5	5.0	1.605380	0.1264550	1.068932E-02	5.6213439E-02
0.001	-2.0	1.0	0.7	2.0	5.0	1.343850	0.2230456	6.943691E-03	3.0303188E-02
0.001	-2.0	0.4472136	0.7	2.0	5.0	1.511812	0.2091396	9.4556569E-03	4.8117992E-02
0.001	-2.0	0.20	0.7	2.0	5.0	1.603936	0.1288501	1.0677759E-02	5.6103650E-02
0.001	-2.0	8.9442730E-02	0.7	2.0	5.0	1.631496	7.1102999E-02	1.0990239E-02	5.8275975E-02
0.001	-2.0	0.04	0.7	2.0	5.0	1.638551	4.2198259E-02	1.1060148E-02	5.8808673E-02
0.001	-2.0	1.7888544E-02	0.7	2.0	5.0	1.640501	2.8907383E-02	1.1076888E-02	5.8952093E-02
0.001	-2.0	8.0000004E-03	0.7	2.0	5.0	1.641110	2.2921769E-02	1.108057E-02	5.8994900E-02
0.001	-2.0	3.5777090E-03	0.7	2.0	5.0	1.641341	2.0237217E-02	1.108218E-02	5.9011355E-02
0.001	-2.0	1.600000E-03	0.7	2.0	5.0	1.641421	1.9038064E-02	1.1081953E-02	5.9016157E-02
0.001	-2.0	7.1554177E-04	0.7	2.0	5.0	1.641455	1.8494142E-02	1.1081794E-02	5.9018083E-02
0.001	-2.0	3.1999999E-04	0.7	2.0	5.0	1.641478	1.8222623E-02	1.1082190E-02	5.9020042E-02
0.001	-2.0	1.4310835E-04	0.7	2.0	5.0	1.641231	1.7009588E-02	1.1061733E-02	5.8979794E-02
0.001	-2.0	6.4000000E-05	0.7	2.0	5.0	1.632113	-3.31621E-02	1.0582196E-02	5.7823595E-02
0.001	-2.0	2.8621667E-05	0.7	2.0	5.0	1.621780	-0.3850439	2.6399890E-02	7.617060E-02
0.001	-2.0	1.2800000E-05	0.7	2.0	5.0	1.420804	-1.199113	0.1606808	0.2212813
0.001	-2.0	5.7243342E-06	0.7	2.0	5.0	0.8607947	-1.815730	0.4344786	0.4906113
0.001	-2.0	2.5600000E-06	0.7	2.0	5.0	0.4170596	-2.013545	0.6878480	0.7248229

Table II : Results for left-handed polarized waves.

δz	γ_m	ν/ω	ω_{pl}/ω	b_l	b_m	$\Re[Z_{m,-}]$	$\Im[Z_{m,-}]$	ρ_v	ρ_w
cm	cm^{-2}	—	—	cm^{-1}	cm^{-1}	—	—	—	—
0.002	-0.10	1.0	0.4	2.0	5.0	1.023569	-0.2220418	2.5559660E-02	1.2030995E-02
0.002	-0.10	0.4472136	0.4	2.0	5.0	0.6082340	-2.404990E-02	0.1386254	5.9551310E-02
0.002	-0.10	0.20	0.4	2.0	5.0	0.3046268	8.7374836E-02	0.3950042	0.2872915
0.002	-0.10	8.9442715E-02	0.4	2.0	5.0	0.1401086	0.1175801	0.6571540	0.5733836
0.002	-0.10	0.04	0.4	2.0	5.0	6.3027918E-02	0.1240501	0.8284824	0.7798951
0.002	-0.10	1.0	0.7	2.0	5.0	1.204453	4.5221075E-02	2.7443613E-03	9.0187080E-03
0.002	-0.30	1.0	0.7	2.0	5.0	1.193522	4.7877148E-02	3.2542401E-03	8.2560228E-03
0.002	-0.50	1.0	0.7	2.0	5.0	1.180051	4.4212595E-02	3.8453243E-03	7.2294935E-03
0.002	-0.70	1.0	0.7	2.0	5.0	1.160175	4.1479744E-02	4.8899553E-03	5.8646179E-03
0.002	-0.90	1.0	0.7	2.0	5.0	1.139820	4.4480190E-02	6.2096985E-03	4.6996060E-03
0.002	-1.1	1.0	0.7	2.0	5.0	1.124310	4.8607107E-02	7.3675248E-03	3.9458331E-03
0.002	-1.3	1.0	0.7	2.0	5.0	1.110216	4.8327602E-02	8.4521407E-03	3.2507351E-03
0.002	-1.5	1.0	0.7	2.0	5.0	1.092046	4.6065655E-02	9.9569010E-03	2.4195234E-03
0.002	-1.7	1.0	0.7	2.0	5.0	1.071431	4.7063630E-02	1.1914670E-02	1.7044590E-03
0.002	-1.9	1.0	0.7	2.0	5.0	1.053238	5.0243363E-02	1.3861340E-02	1.2703417E-03
0.002	-2.1	1.0	0.7	2.0	5.0	1.036763	5.1144626E-02	1.5743461E-02	9.5573813E-04
0.002	-2.3	1.0	0.7	2.0	5.0	1.017931	5.0243929E-02	1.8043717E-02	6.9847575E-04
0.002	-2.5	1.0	0.7	2.0	5.0	0.9971426	5.1166266E-02	2.0854885E-02	6.5798615E-04
0.002	-2.7	1.0	0.7	2.0	5.0	0.9775501	5.3486634E-02	2.3771502E-02	8.5978274E-04
0.002	-2.9	1.0	0.7	2.0	5.0	0.9586307	5.4436885E-02	2.6794586E-02	1.2176490E-03
0.002	-3.1	1.0	0.7	2.0	5.0	0.9379798	5.4664586E-02	3.0348474E-02	1.8183473E-03
0.002	-3.3	1.0	0.7	2.0	5.0	0.9163655	5.6155324E-02	3.4411564E-02	2.7609433E-03
0.002	-3.5	1.0	0.7	2.0	5.0	0.8953046	5.7973005E-02	3.8707890E-02	3.9832653E-03
0.002	-3.7	1.0	0.7	2.0	5.0	0.8737445	5.9011023E-02	4.3441374E-02	5.5266153E-03
0.002	-3.9	1.0	0.7	2.0	5.0	0.8509362	6.0323611E-02	4.8863396E-02	7.5399219E-03
0.002	-0.10	0.20	0.7	2.0	5.0	1.530437	-0.4018503	2.4216706E-02	6.7459881E-02
0.002	-0.30	0.20	0.7	2.0	5.0	0.9198043	-0.2962551	4.9635164E-02	2.4963710E-02
0.002	-0.50	0.20	0.7	2.0	5.0	0.8173683	0.1299708	6.0310688E-02	1.5135841E-02
0.002	-0.70	0.20	0.7	2.0	5.0	1.183372	0.4286596	3.1557865E-02	4.3906346E-02
0.002	-0.90	0.20	0.7	2.0	5.0	1.585835	-8.671013E-02	8.6234715E-03	5.2392937E-02
0.002	-1.1	0.20	0.7	2.0	5.0	1.019531	-0.3418373	3.7770782E-02	2.7943783E-02
0.002	-1.3	0.20	0.7	2.0	5.0	0.7858384	1.6170604E-02	6.6066355E-02	1.4462125E-02
0.002	-1.5	0.20	0.7	2.0	5.0	1.021792	0.3385211	3.7067436E-02	2.7383350E-02
0.002	-1.7	0.20	0.7	2.0	5.0	1.431224	6.6990713E-03	1.3700196E-03	3.1467170E-02
0.002	-1.9	0.20	0.7	2.0	5.0	0.9832748	-0.2831434	3.6823947E-02	2.0044589E-02
0.002	-2.1	0.20	0.7	2.0	5.0	0.7682865	3.0751402E-02	7.1726531E-02	1.7468214E-02
0.002	-2.3	0.20	0.7	2.0	5.0	1.016011	0.2812443	3.1764485E-02	1.9152079E-02
0.002	-2.5	0.20	0.7	2.0	5.0	1.241155	-9.764470E-02	2.6143866E-03	1.3451104E-02
0.002	-2.7	0.20	0.7	2.0	5.0	0.8327137	-0.1692217	5.8518685E-02	1.6714709E-02
0.002	-2.9	0.20	0.7	2.0	5.0	0.7810879	0.1316488	7.1088627E-02	2.0458298E-02
0.002	-3.1	0.20	0.7	2.0	5.0	1.093105	0.1396070	1.2783808E-02	6.3988375E-03
0.002	-3.3	0.20	0.7	2.0	5.0	0.9242671	-0.1738878	3.8026121E-02	9.6362308E-03
0.002	-3.5	0.20	0.7	2.0	5.0	0.7225468	2.5549777E-02	8.7579750E-02	2.6158277E-02
0.002	-3.7	0.20	0.7	2.0	5.0	0.9211278	0.1504872	3.7198171E-02	7.7738422E-03
0.002	-3.9	0.20	0.7	2.0	5.0	0.8900723	-0.1142369	4.1701272E-02	7.0100999E-03

$$N = D(-k_1 z_1)O_1 D(-k_2 d_c)O_2 D(-k_3 d_d)O_3 D(-k_2 d_c)O_4 D(k_1 z_4) \qquad (A.3)$$

Note that the actual thickness of the layers appears in the three D's sandwiched between the O's. Computation of N elements is easy, and simple diagram techniques may be used. The results can be further simplified by noting that

$$q_{4+} = k_4 + k_5 = k_2 + k_1 = q_{1+} \qquad q_{3+} = q_{2+} \qquad q_{4-} = k_4 - k_5 = k_2 - k_1 = -q_{1-} \qquad q_{3-} = -q_{2-}$$
$$(A.4)$$

The first element of N is given by $n_{11} = \exp(-ik_1 d_d - 2ik_1 d_c)\Delta/(16k_1 k_2 k_3 k_4)$ where

$$\Delta = e^{-ik_3 d_d}(q_{1-}q_{2-}e^{ik_2 d_c} + q_{1+}q_{2+}e^{ik_2 d_c})^2 - e^{ik_3 d_d}(q_{1-}q_{2+}e^{ik_2 d_c} + q_{1+}q_{2-}e^{ik_2 d_c})^2 \quad (A.5)$$

Reflection and transmission may be found by the coefficient:

$$\alpha_5 = \frac{16k_1 k_2^2 k_3}{\Delta} e^{-ik_1 d_d - 2ik_1 d_c} \qquad (A.6)$$

$$\beta_1 = -2ie^{-2ik_1 d_d - 4ik_1 d_c} \times$$

$$\frac{q_{1-}q_{1+}[q_{2+}^2 \sin(k_3 d_d + 2k_2 d_c) + q_{2-}^2 \sin(k_3 d_d - 2k_2 d_c)] + q_{2-}q_{2+}[q_{1-}^2 + q_{1+}^2]\sin(k_3 d_d)}{\Delta}$$
$$(A.7)$$

since k_1 is real, the exponential factor does not affect ρ and T.

As regards to the other amplitudes, we find (with the shorthand $d_h = d_d/2$)

$$\alpha_4 = \frac{8k_1 k_2 k_3 q_{1+}}{\Delta} e^{-iq_{1+}(d_c + d_h)} \qquad (A.8)$$

$$\beta_4 = -\frac{8k_1 k_2 k_3 q_{1-}}{\Delta} e^{-iq_{1-}(d_c + d_h)} \qquad (A.9)$$

$$\alpha_3 = 4k_1 k_2 \frac{q_{1+}q_{2+}e^{-ik_2 d_c} + q_{1-}q_{2-}e^{ik_2 d_c}}{\Delta} e^{-ik_1 d_c - i(k_1 + k_3)d_h} \qquad (A.10)$$

$$\beta_3 = -4k_1 k_2 \frac{q_{1+}q_{2-}e^{-ik_2 d_c} + q_{1-}q_{2+}e^{ik_2 d_c}}{\Delta} e^{-ik_1 d_c - i(k_1 - k_3)d_h} \qquad (A.11)$$

$$\alpha_2 = 2k_1 \frac{-2iq_{1-}q_{2-}q_{2+}\sin(k_3 d_d)e^{ik_2 d_c} + q_{1+}[q_{2+}^2 e^{ik_3 d_d} - q_{2-}^2 e^{-ik_3 d_d}]e^{-ik_2 d_c}}{\Delta} e^{-ik_1 d_c - id_h q_{1-}}$$
$$(A.12)$$

$$\beta_2 = 2k_1 \frac{-2iq_{1+}q_{2-}q_{2+}\sin(k_3 d_d)e^{-ik_2 d_c}q_{1-}[q_{2+}^2 e^{ik_3 d_d} - q_{2-}^2 e^{-ik_3 d_d}]e^{ik_2 d_c}}{\Delta} e^{-ik_1 d_c - id_h q_{1+}}$$
$$(A.13)$$

Note that the expressions in square brackets of eqs. (A.12) and (A.13) are identical.

From eq. 34, performing the integration on the required regions $z_1 \leq z \leq z_2$ and $z_3 \leq z \leq z_4$ and remembering z_i definitions (see 7), we get the dissipated power inside the two metallic layers:

$$D_c = \frac{\sigma \omega P_{in}}{2k_1}\left[\frac{sh(k_2'' d_c)}{k_2''}\left\{(|\alpha_2|^2 + |\beta_4|^2)e^{k_2''(d_d + d_c)} + (|\alpha_4|^2 + |\beta_2|^2)e^{-k_2'(d_d + d_c)}\right\} + \right.$$

$$2\frac{\sin(k_2' d_c)}{k_2'} \mathrm{Re}\left\{(\alpha_2\beta_2^* + \alpha_2^*\beta_2)\mathrm{e}^{-ik_2'(d_d+d_c)}\right\}\Bigg] \qquad (A.14)$$

Note that, even if α and β appear squared here, the last exponential factor of each equation from (A.7) to (A.13) does matter: first, these factors are not unimodular, since the k 's have imaginary part; second, these factors contain the relative phase between α and β which affects the second line of (A.14) . Anyway, several exponentials cancel between (A.7) - (A.13) and (A.14) .

Similarly, the power dissipated in the dielectric is

$$D_d = \frac{\sigma_d \omega P_{\mathrm{in}}}{2k_1}\left[\frac{\mathrm{sh}(k_3''d_d)}{k_3''}\left\{(|\alpha_3|^2 + |\beta_3|^2) + 2\frac{\sin(k_3'd_d)}{k_3'}\mathrm{Re}(\alpha_3\beta_3^*)\right\}\right] \qquad (A.15)$$

where the effective conductivity is $\sigma_d = \omega\epsilon_0\epsilon_r\tan\delta$.

ACKNOWLEDGMENTS

REFERENCES

[1] B.Jacquot, P.Briand, F.Bourg and R.Geller, *Nucl. Instr. Meth.*, **A269**, 1.

[2] M.Cavenago, G.Bisoffi, *Nucl. Instr. Meth.* **301 A**, 9 (1991).

[3] G.L. Ragan, *Microwave Transmission Circuits*, (McGraw-Hill, New York, 1948)

[4] N. Marcuwitz,*Waveguide Handbook*, (McGraw-Hill, New York, 1951)

[5] R.G. Carter *Electromagnetic waves*, Chapman and Hall, London, (1990).

[6] C.T.Iatrou and M.Cavenago, " Field analysis of rectangular waveguide open-junctions", submitted to *IEEE Trans. on Micr. Theory and Tech.*

[7] V.Bechtold, H.Dohrmann, S.A. Sheikh, "A highly efficient ECR ion source for radioactive beams", in *Contributed Papers of the 7th Workshop on ECR Ion Sources*, p.248-260, (ed. H. Beuscher, Jul-Conf-57, KernForschungAnlage Julich, 1986)

[8] H.Beuscher, private communication.

[9] J.C.Pivin, G.Della Mea, V.Rigato, M.Toninandel, S.Carturan, "Hardness and adhesion of ion implanted polyimides ", to be published in . *Nucl. Instr. Meth. B*, Proceedings of 7th Int. Conf. on Radiation Effects in Insulators (6-10 Sept 93, Nagoya).

[11] G.Mourier, private communication.

[10] *OPERA reference manual (including TOSCA)*, by Vector Fields Limited, Oxford (version 2.2, June 1992).

[12] Y. Torij et al., *Rev. Sci. Instr.*, **61**, 253, (1990).

[14] D.G. Swanson, *Plasma waves*, especially p. 101. (Academic Press, San Diego, 1989).

[13] R.Geller, " Electron heating in ECRIS", p. 1-17 in (ed. A.G. Drentje, Kernfysisch Versneller Institute-Report 996, Groningen, 1993).

[15] K.S. Golovanivsky, "ECRIS plasma: stochastic heating or Langmuir caviton collapses?" in *Proceedings of the 11th Int. Work. on Electron Cyclotron Resonance Ion Source (ECRIS11)*, p. 78-84 Ref. 13.

FIGURE CAPTIONS

1) The microwave circuit for the ECR Alice. Power is divided into two lines. Note the two alternative concepts for DC-break.

2) The demountable DC break, opened, but not completely disconnected from the ion source cooling circuit; note the collar-like disposition of cooled parts (oxidized copper is rendered as black) and the standard choke flange of the connecting waveguide (clean brass is more shiny).

3) Currents on the waveguide wall at the cut.

4) Choke flange machining parameters; we add w_t,R_o and r_r to the standard choke to better adapt to a DC-break.

5) Choke flange schematic: impedances and port labels are defined.

6) The new DC break; choke is slightly modified and alignment is guaranteed by plexiglas enclosure. Eventual sparks can be observed.

7) The 1D-model for metallized windows.

8) Transmission τ (solid line) and reflection coefficient ρ (dashed line) through a 1 mm teflon sheet, covered with material of conductivity $\sigma = 1$ mho/m and thickness d_c on each side; conduction loss coefficient A_c (dotted line) is also shown.

9) As in Fig. 9 but $\sigma = 1000$ mho/m.

10) Transmission coefficient τ as a function of surface conductivity σd_c (front axis) and of bulk conductivity σ (profundity axis).

11) As in Fig. 10 , but plotting reflection ρ ..

12) As in Fig. 10 , but plotting a ; spikes (up to 1600 ohm) due to numerical errors in upper left corner were edited.

13) Electrostatic fields on the major symmetry axis of the guide section, in the teflon side facing the choke flange. Showing the potential V and the field E_x , E_z in the limit $z \to 0^+$ on the line $y = a/2$ as a function of $x' = x - a$. Note that $E_y = 0$.

14) As in Fig. 13 but in limit $z \to d^-$ (teflon facing the flat flange).

15) Electrostatic fields on a guide diagonal in the teflon side facing the choke flange. Showing the potential V and the field E_x ,E_{para} and E_z on the line $y = x'/2 + a/2$ in the limit $z = 0^+$ as a function of $x' = x - a$.

16) As in Fig. 15 but in the limit $z = d^-$ (teflon facing the flat flange).

17) Section of Alice vacuum chamber.

18) Coupler details: a) refers to coupler A, and with ψ changed, to coupler B; b) refers to coupler C, and with θ changed, to couplers D,E.

19) Impedance and reflection as function of ν/ω (see table I data).

20) Field profile of W_{M+} in the case $\gamma_m = \gamma_M = -2$ cm^{-2}, $\omega_{pl}/\omega = 0.7$, $\nu/\omega = 0.2$, $b_l = 2$ cm^{-1} and $b_m = 5$ cm^{-1} of Table I.

PILOT

rear fan

PANEL

KLYSTRON

P. SUPPLY

RS-232

10 KW

WR62

2 kW 14.4 Ghz

10 db
coupler

350W

200 W 14.4 Ghz

E-H
tuner

200W

bidirectional couplers

level meters

E-H
tuner

E-H
tuner

2 stage

DC cuts

E-H
tuner

WR62

Kapton foil;
indium seals

Alice vacuum chamber

WR62

2nd stage coupler

1ST stage coupler
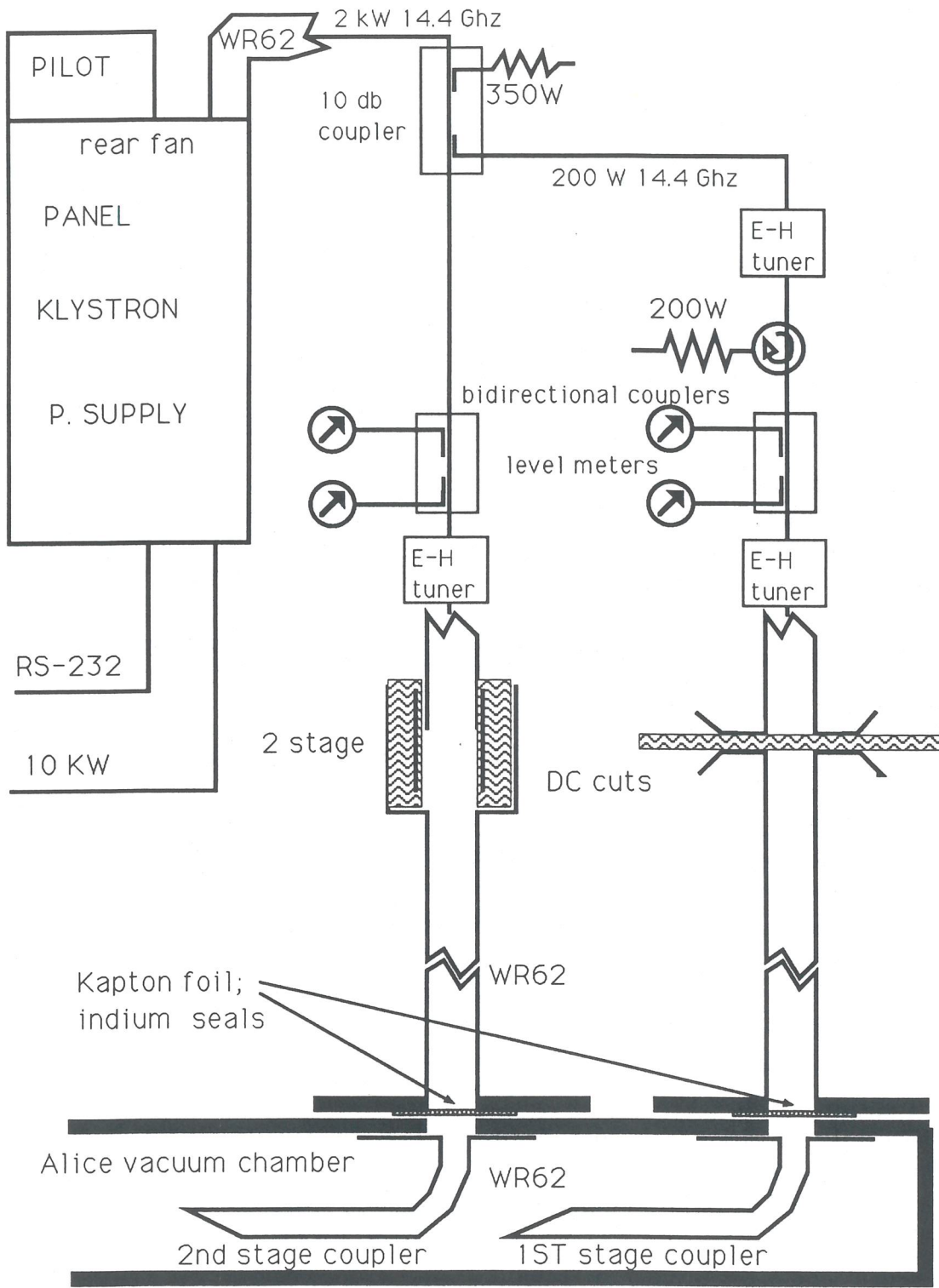
*FIG 1); the microwave
circuit for the Ecr Alice*
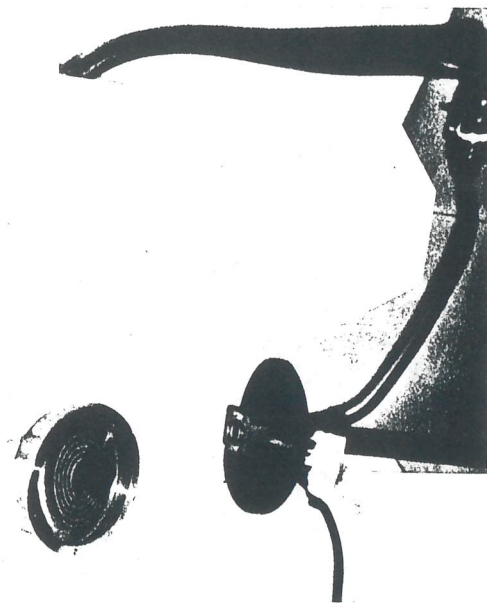
Fig 2) The demountable DC-break
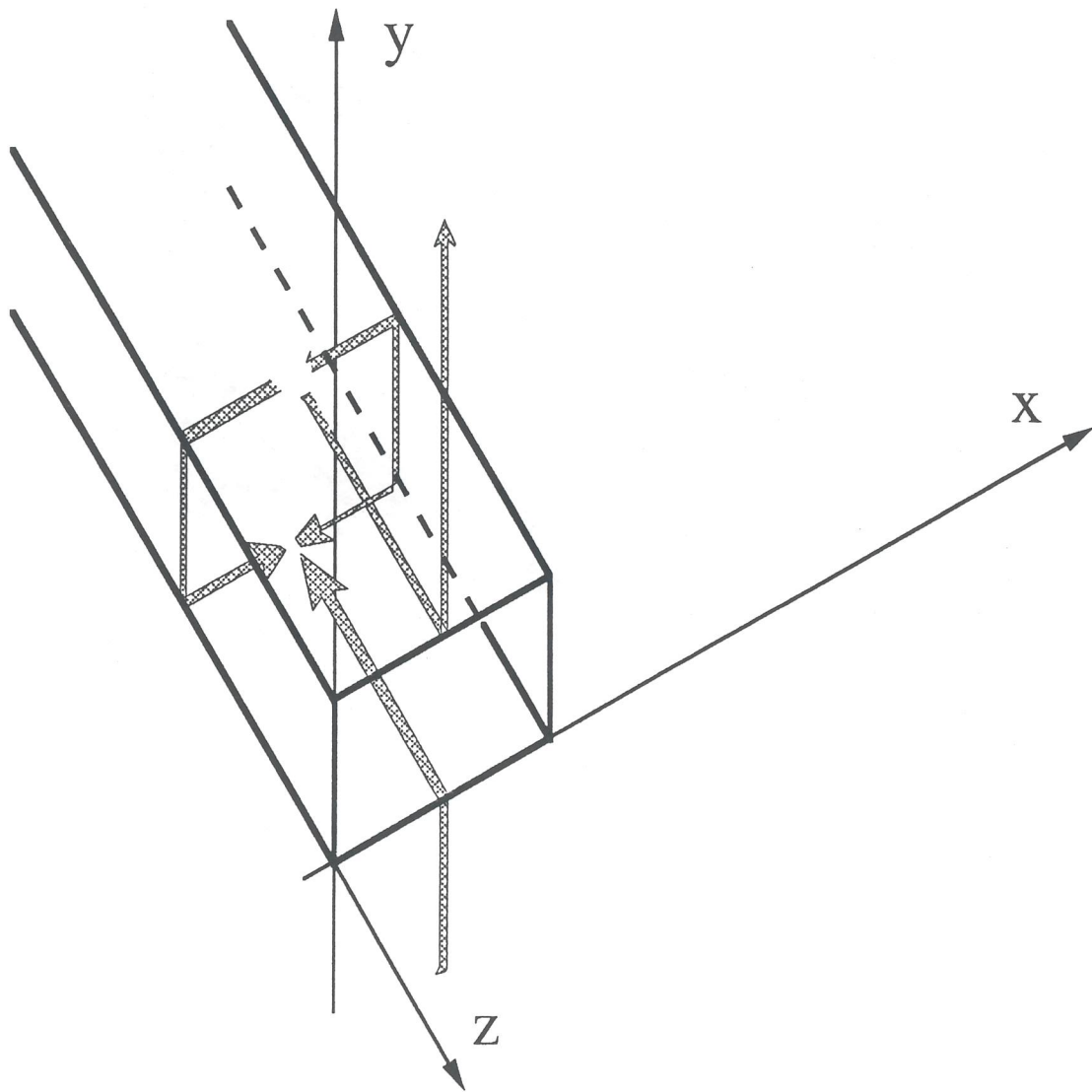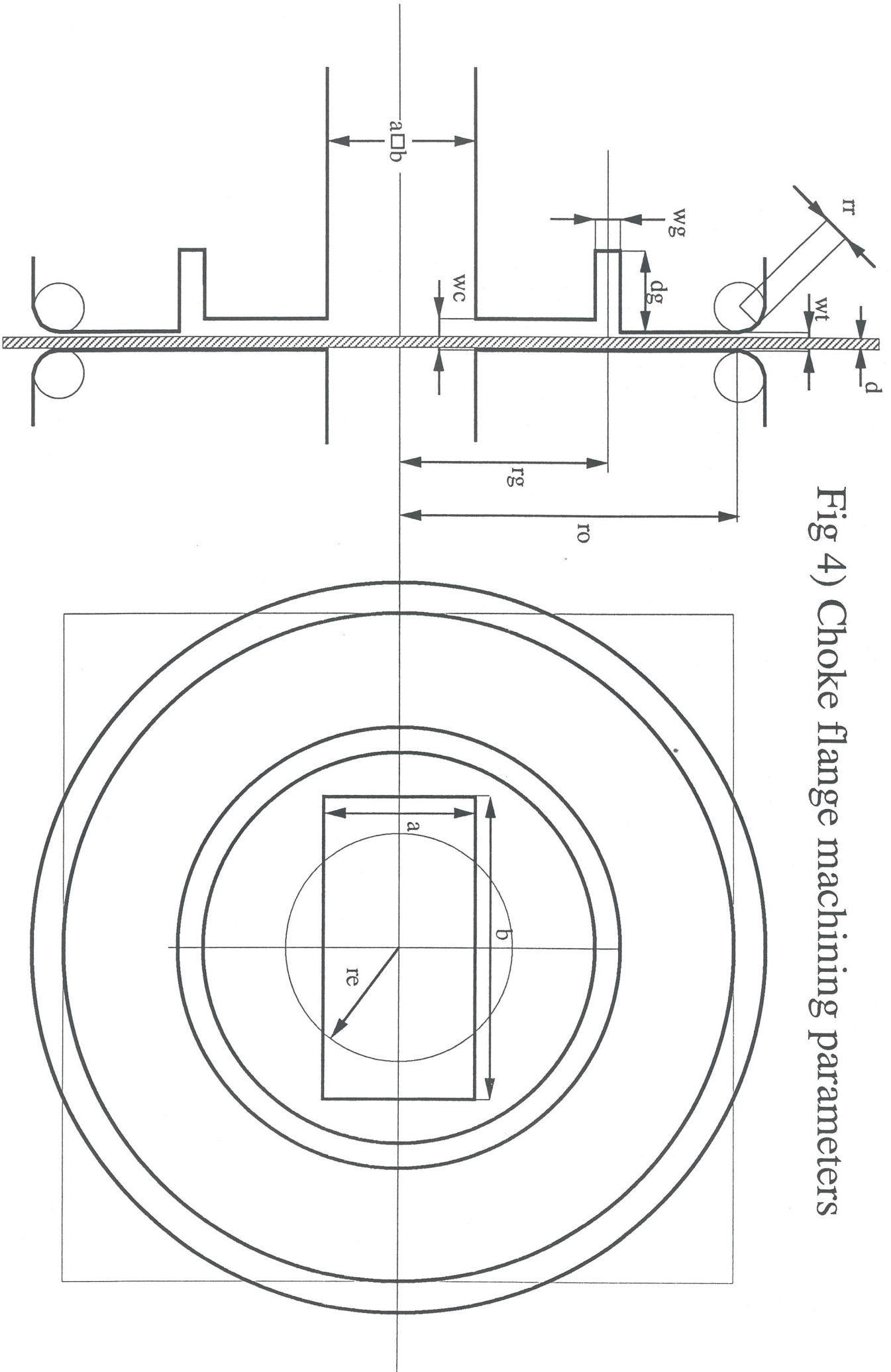
Fig 3) Currents in the
waveguide wall at the cut

Fig 4) Choke flange machining parameters

Zv = 377 Ohm/□

insulation gap

Z2l

Z2o

line 2

Z2i

Z=0 (short)

Zgo Zgi

groove

Z11

Z1o

line or port 1

Z1i

port in   Zin   Zout   Zout   port out

Z1'i

line or port 1'

line 2'
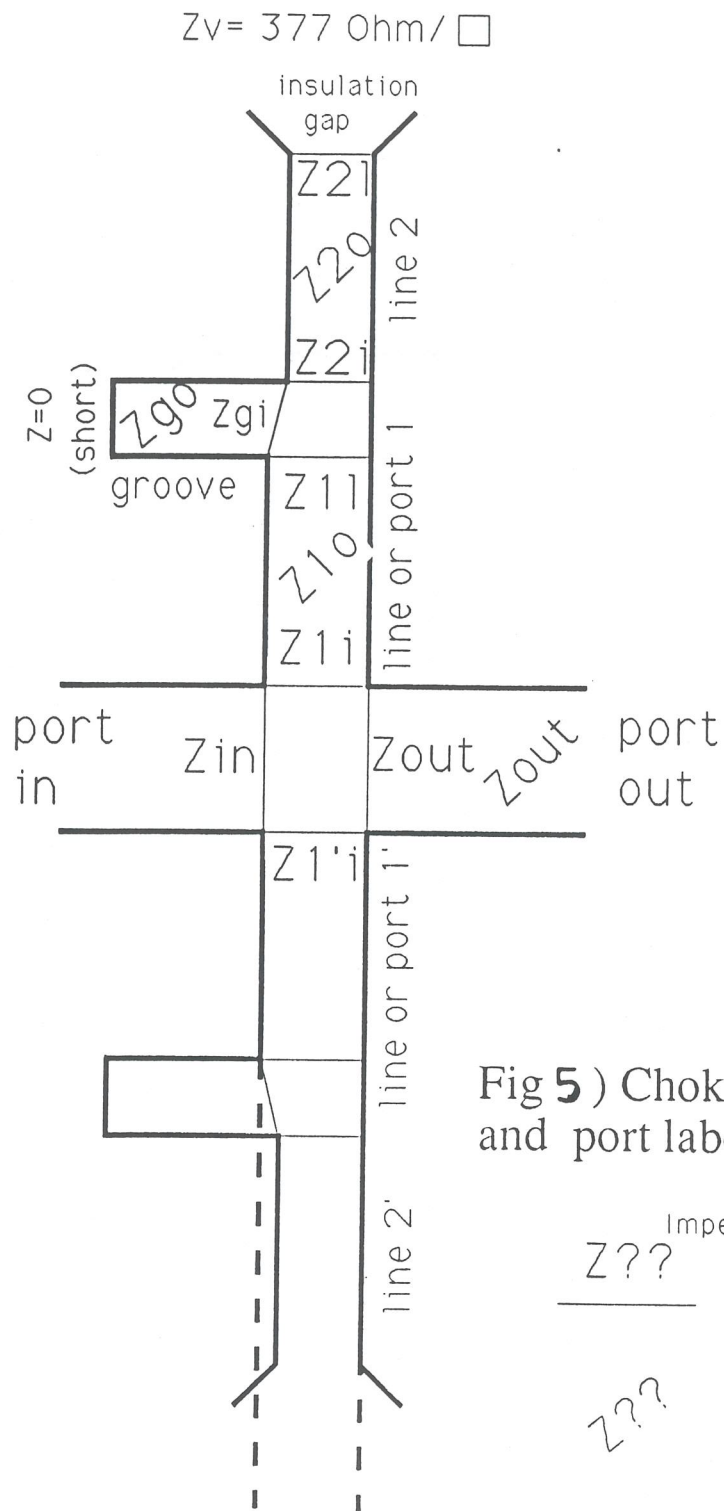
Fig 5) Choke flange schematic: impedance and port labels are defined.

Impedance of the end;

Z??
_____ end of a transmission line;

Z??   impedance of a line.
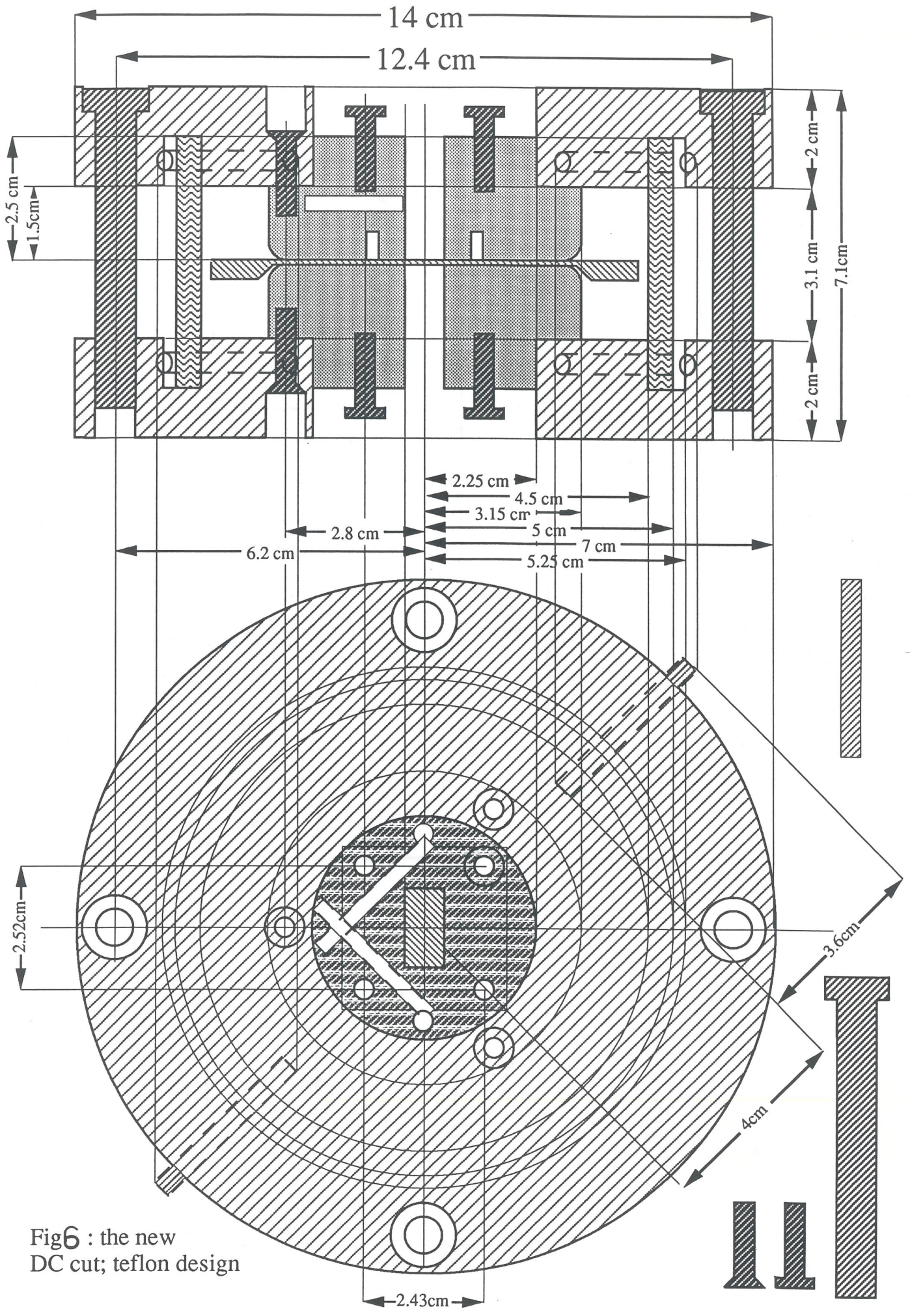
Fig6 : the new
DC cut; teflon design
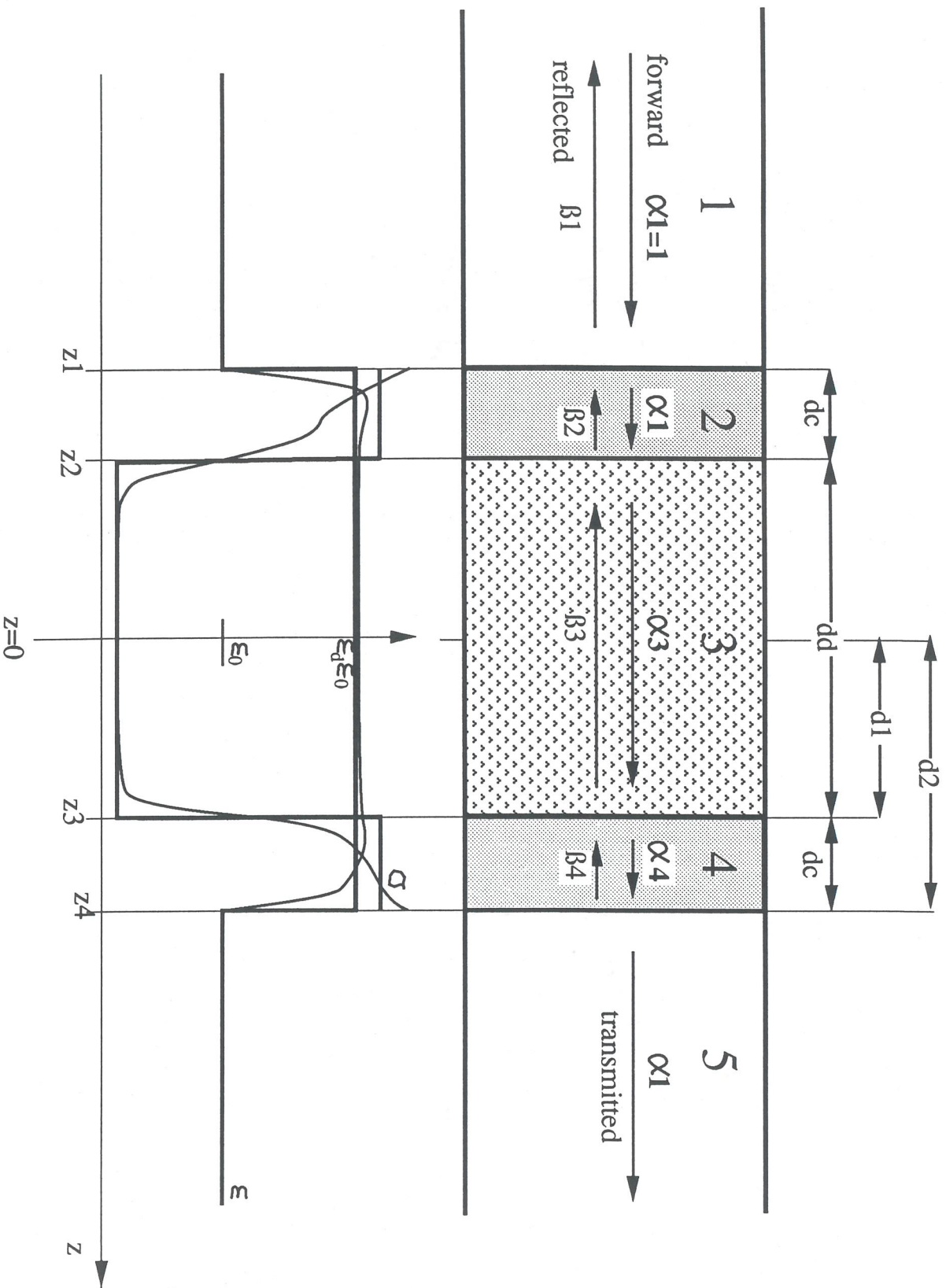
Fig.7: The 1D model for metalized window.
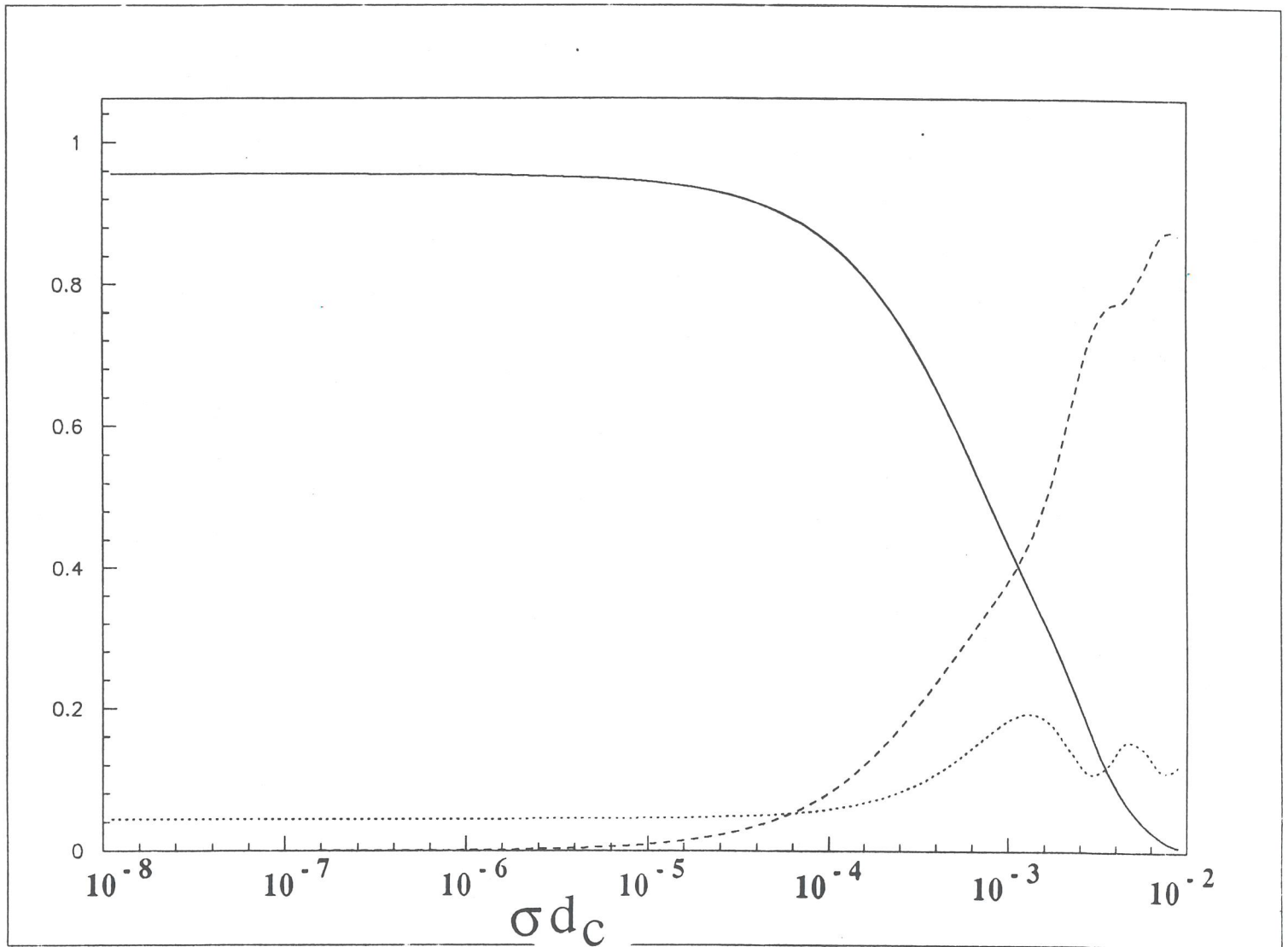
Fig 8) Transmission (solid line), reflection (dashed line), and absorption (dotted line) coefficients for σ =1 mho/m.
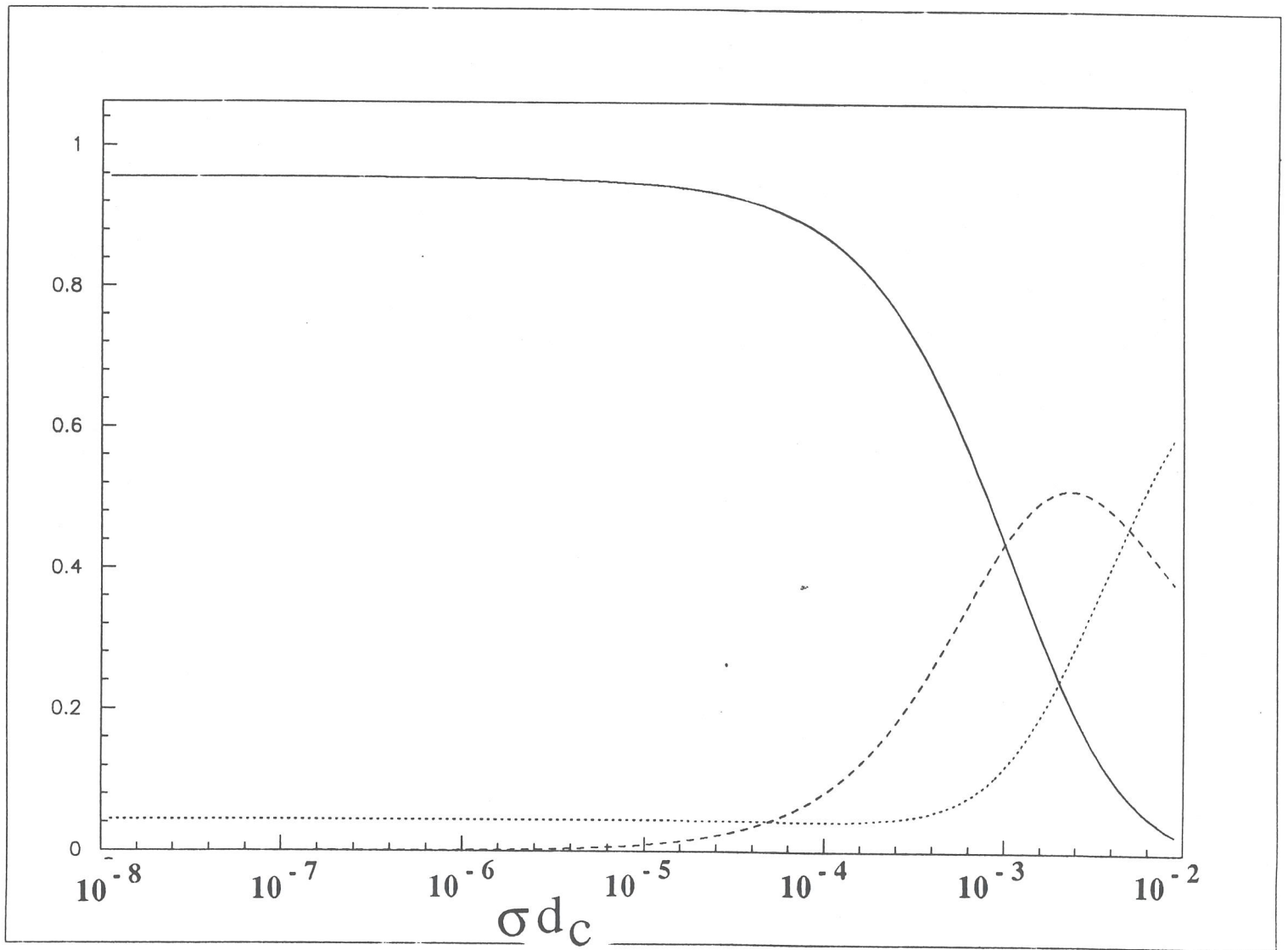
Fig 9) As Fig 8, but σ =1000 mho/m.
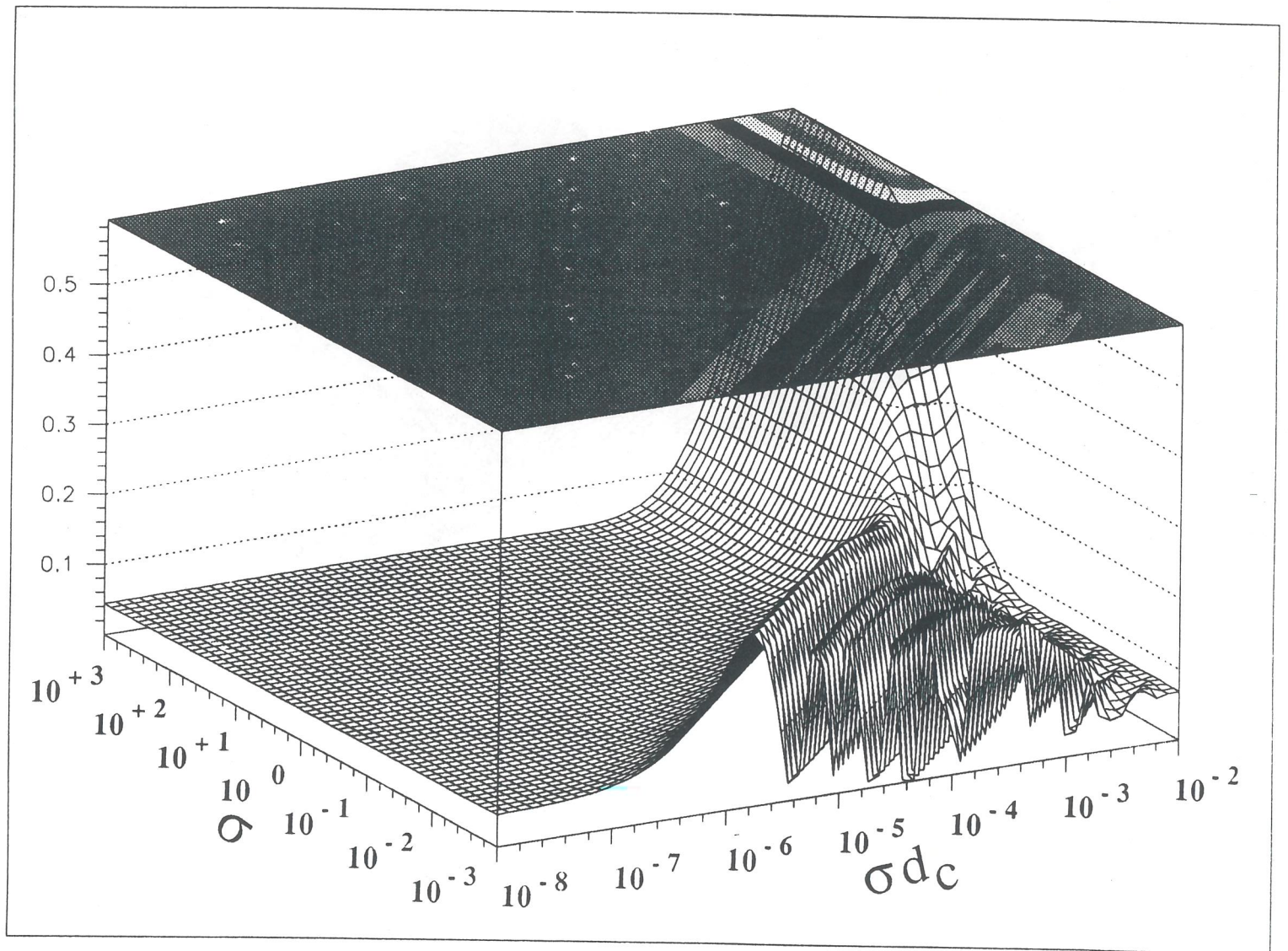
Fig 11) Reflection coefficient.
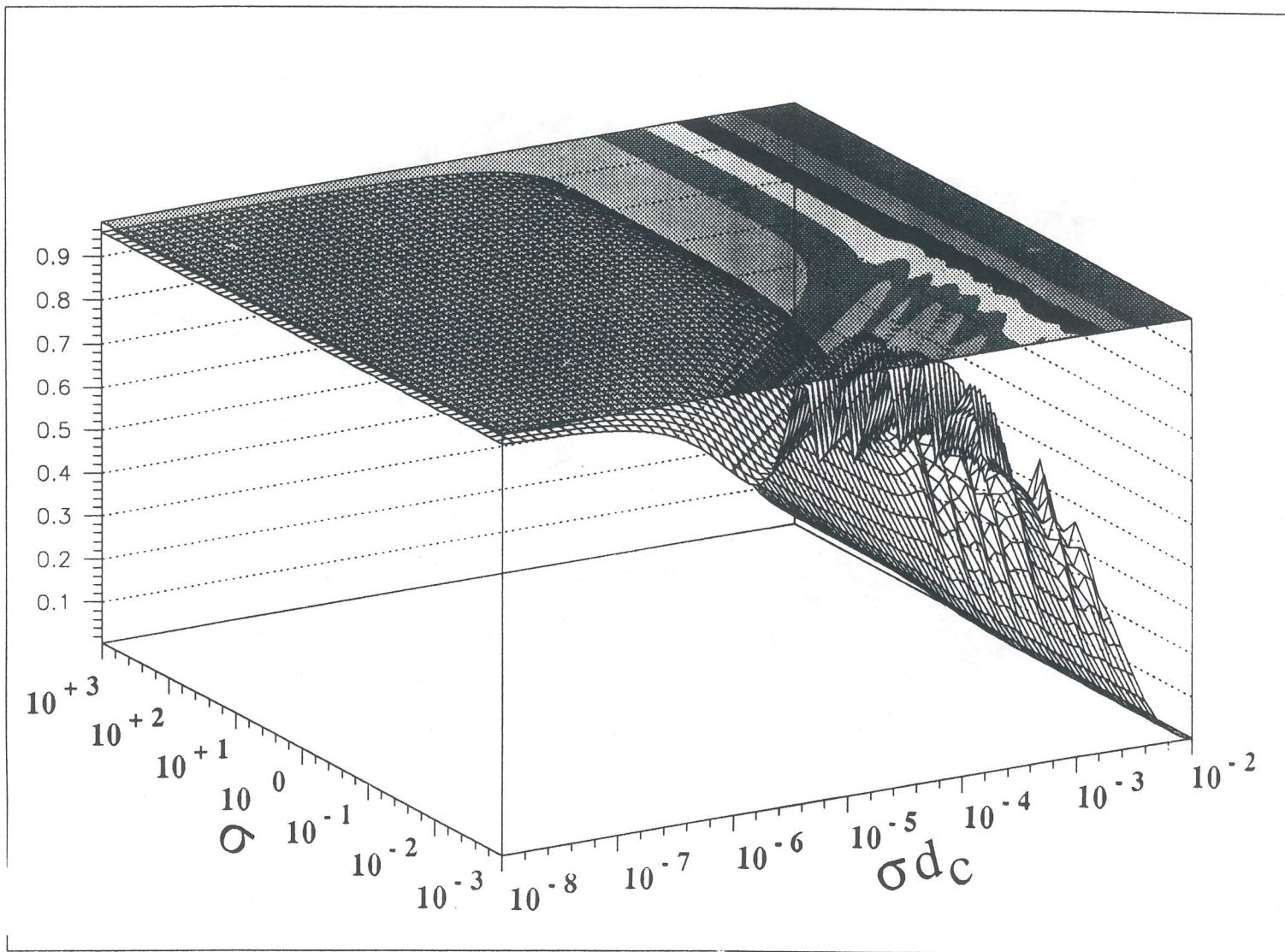
Fig 10) Transmission coefficient
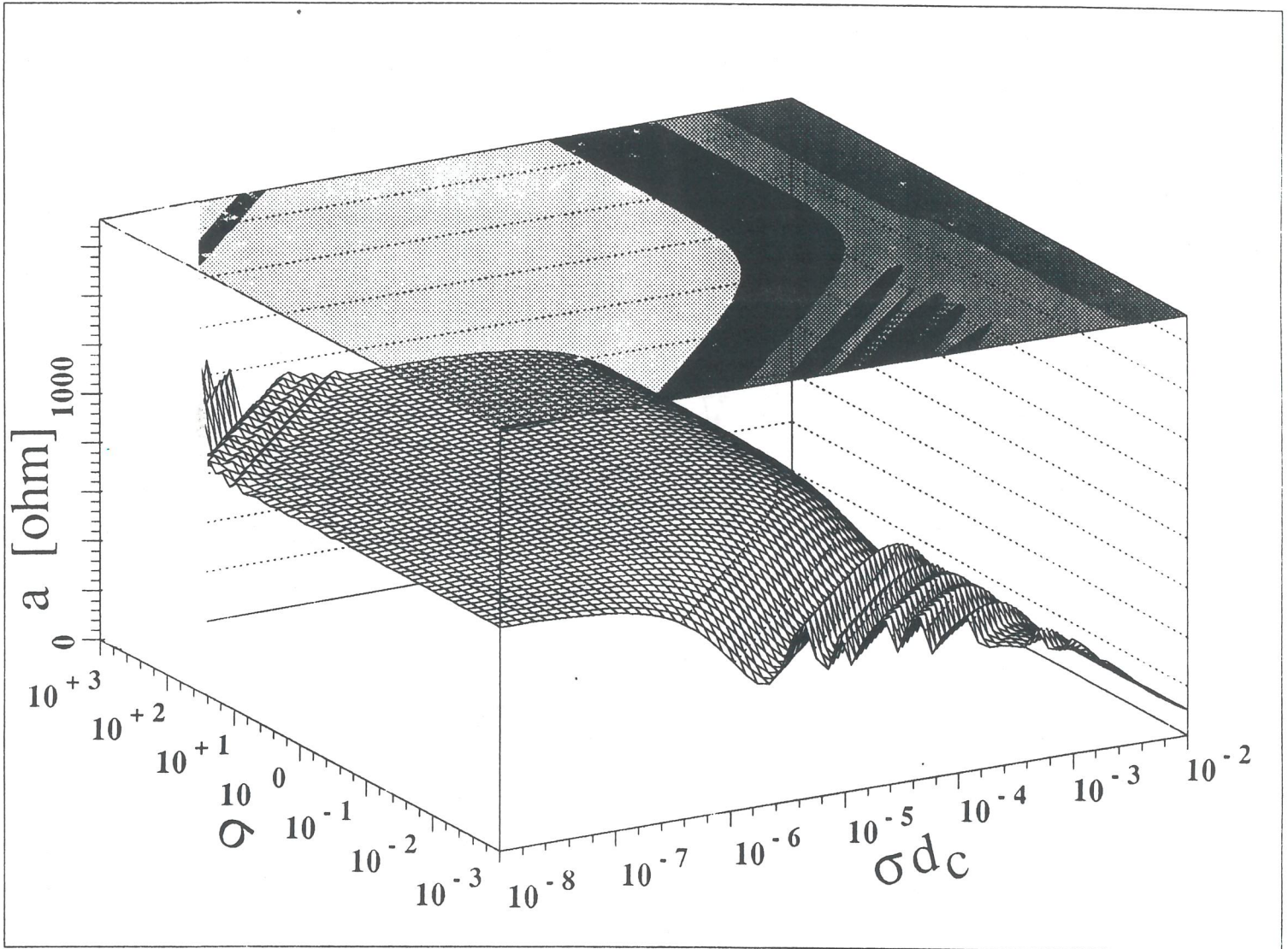
Fig 12) Absorption factor *a*
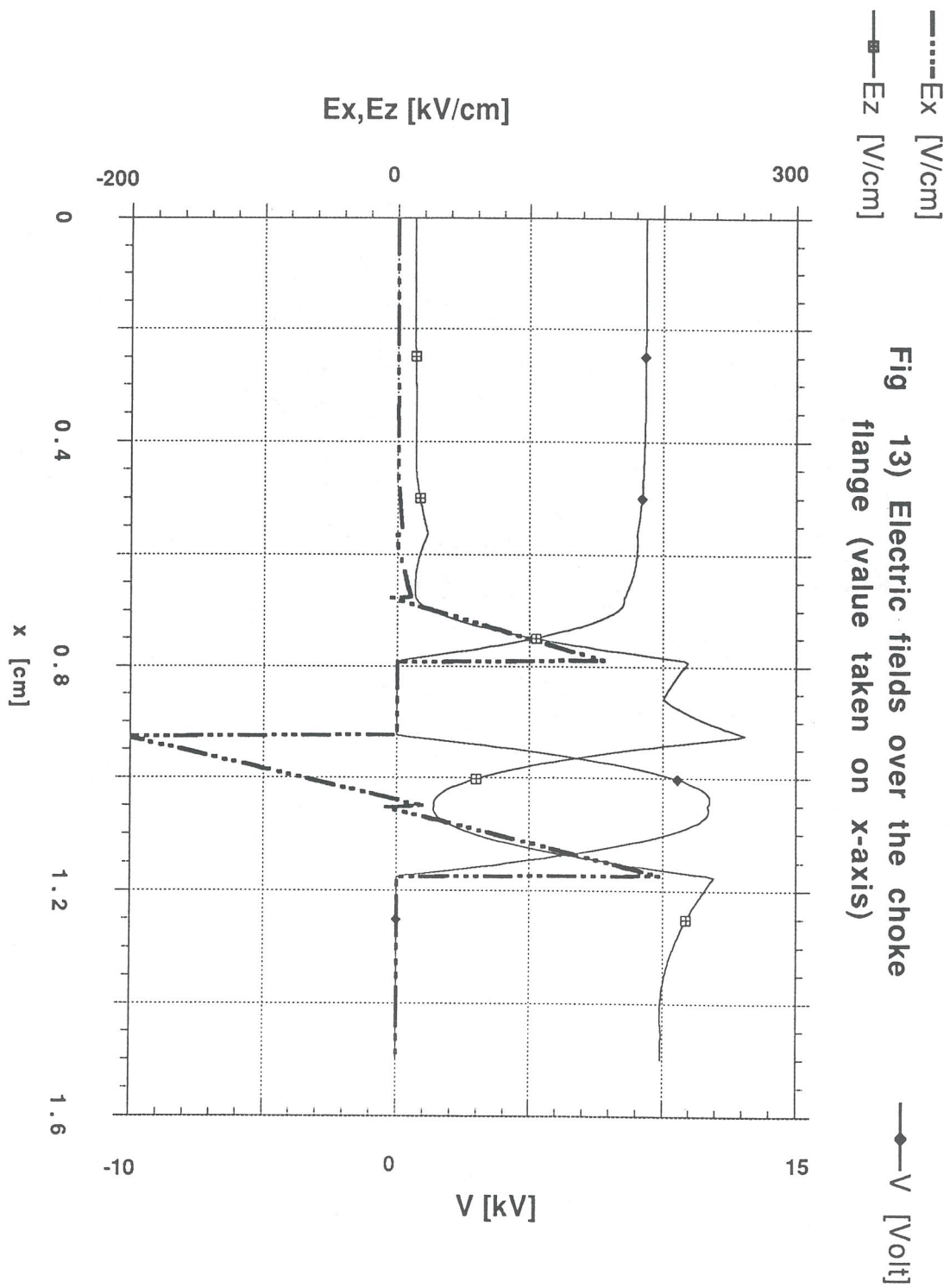
Fig 13) Electric fields over the choke flange (value taken on x-axis)

Fig 14) As in Fig 13, but on the other flange
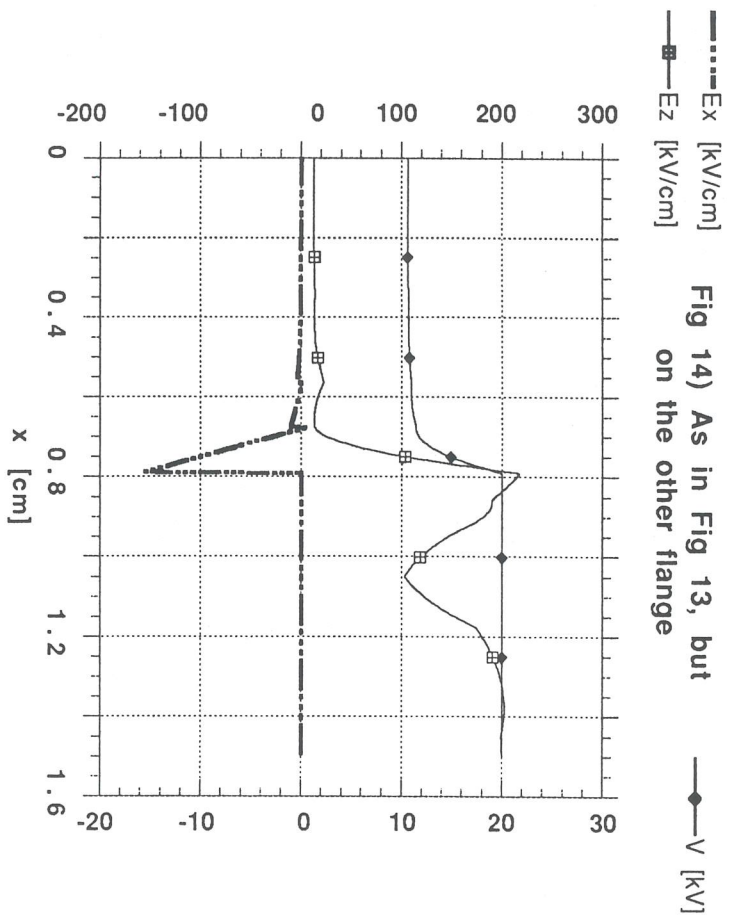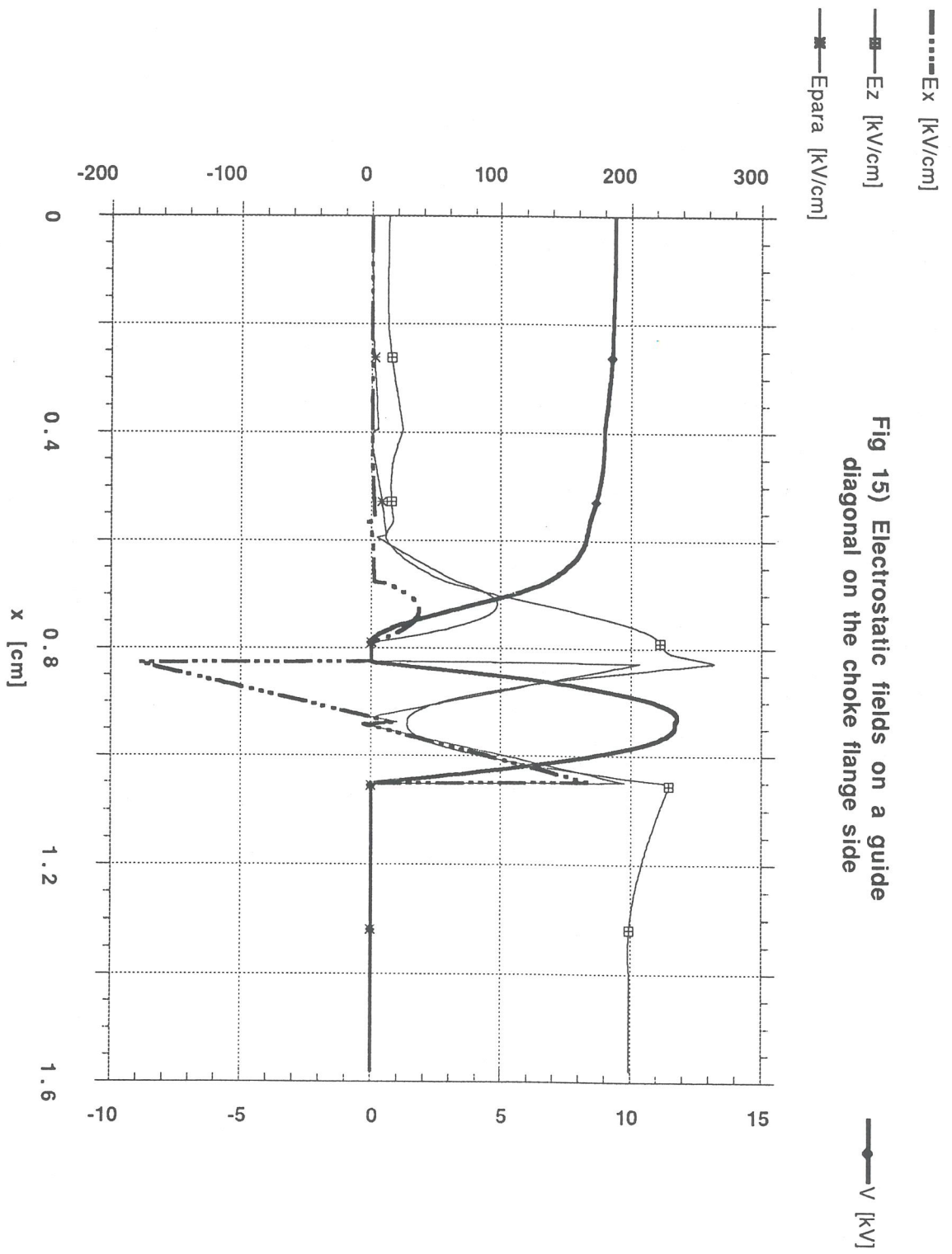
Fig 15) Electrostatic fields on a guide
diagonal on the choke flange side
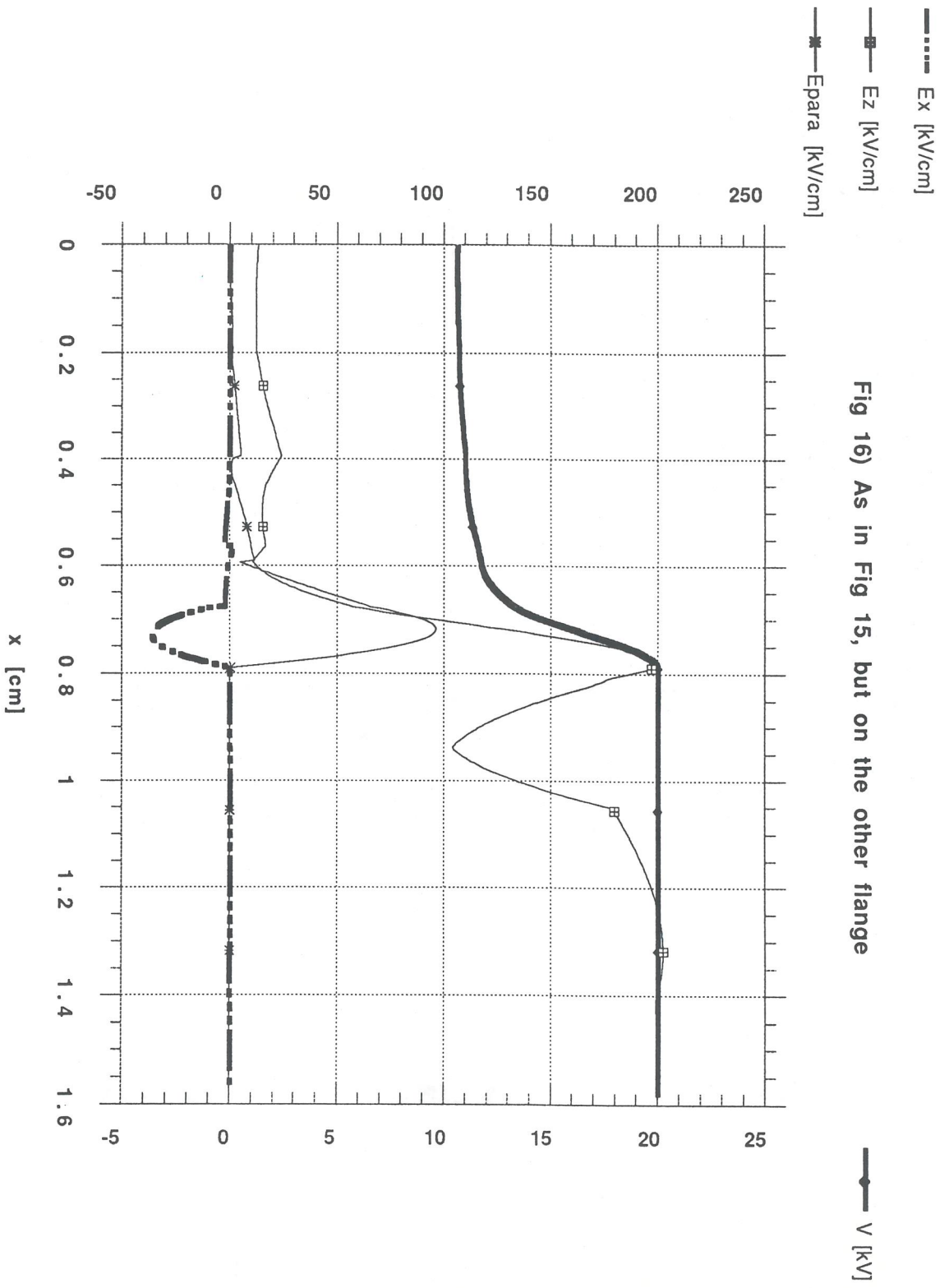
Fig 16) As in Fig 15, but on the other flange

Ex [kV/cm]

Ez [kV/cm]

Epara [kV/cm]

V [kV]

x [cm]

2nd stage

1st stage

rays

y'

Q_1

x'

P_1

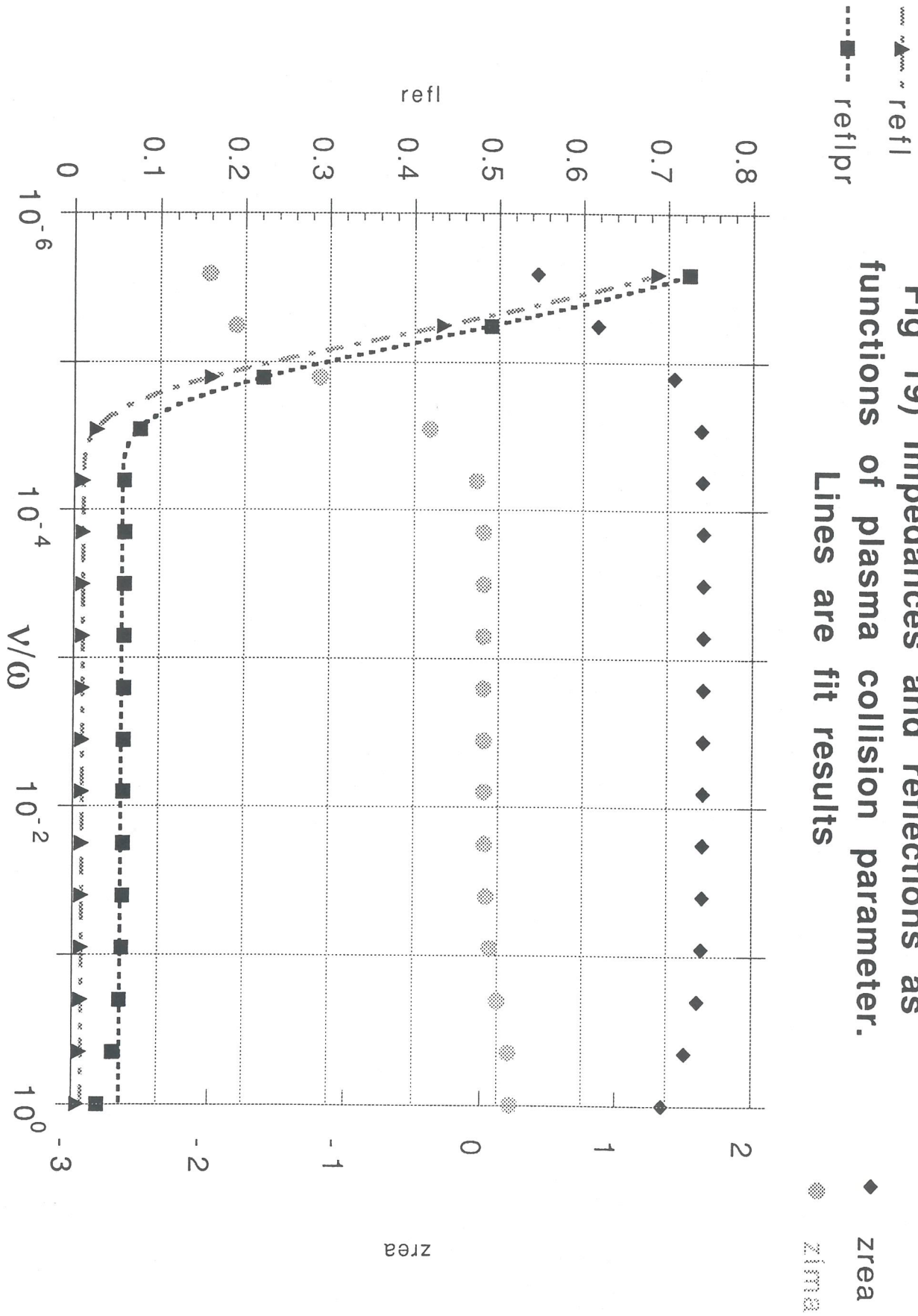Q

0

5 cm
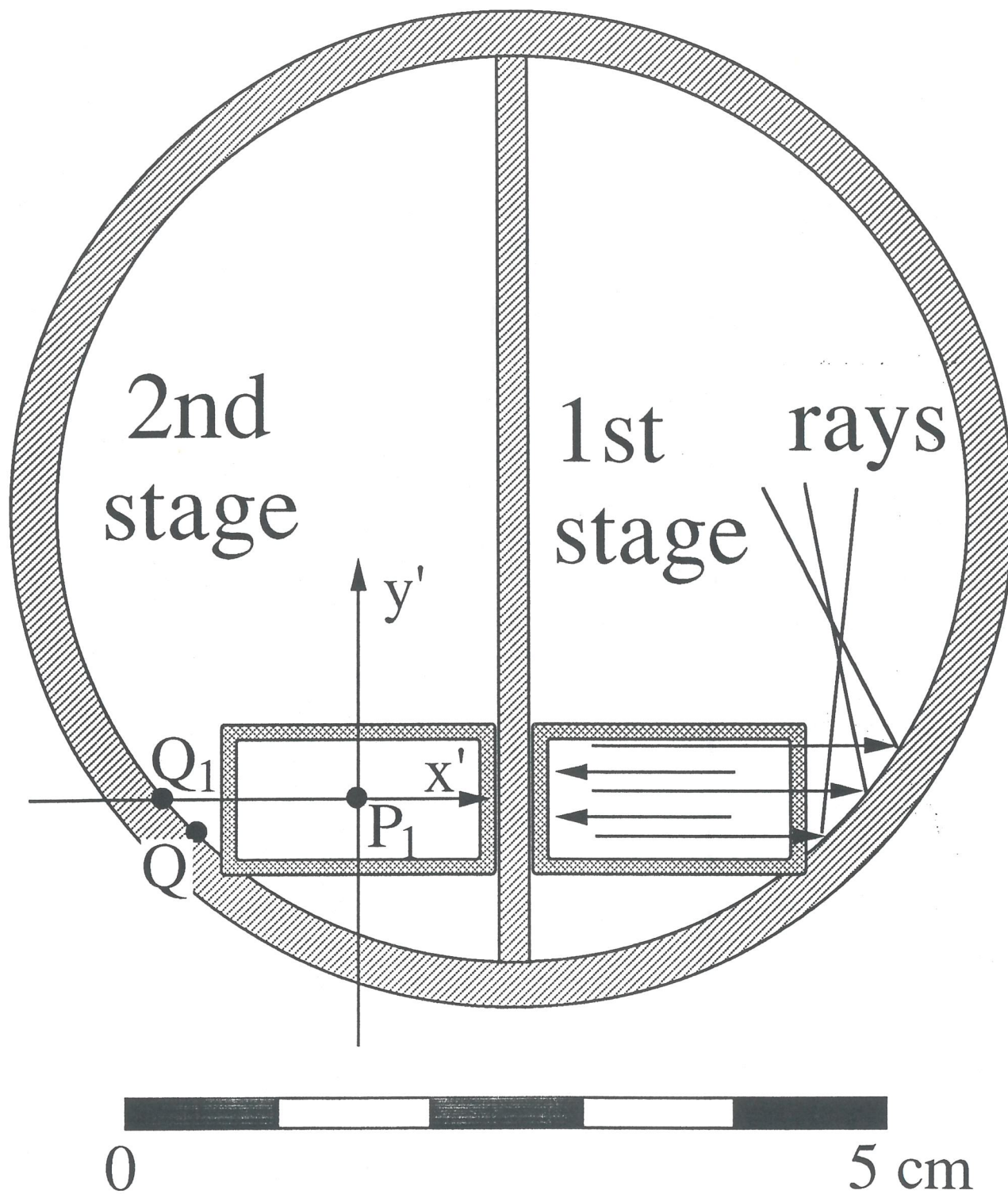
Fig 17) Section of the Alice vacuum chamber
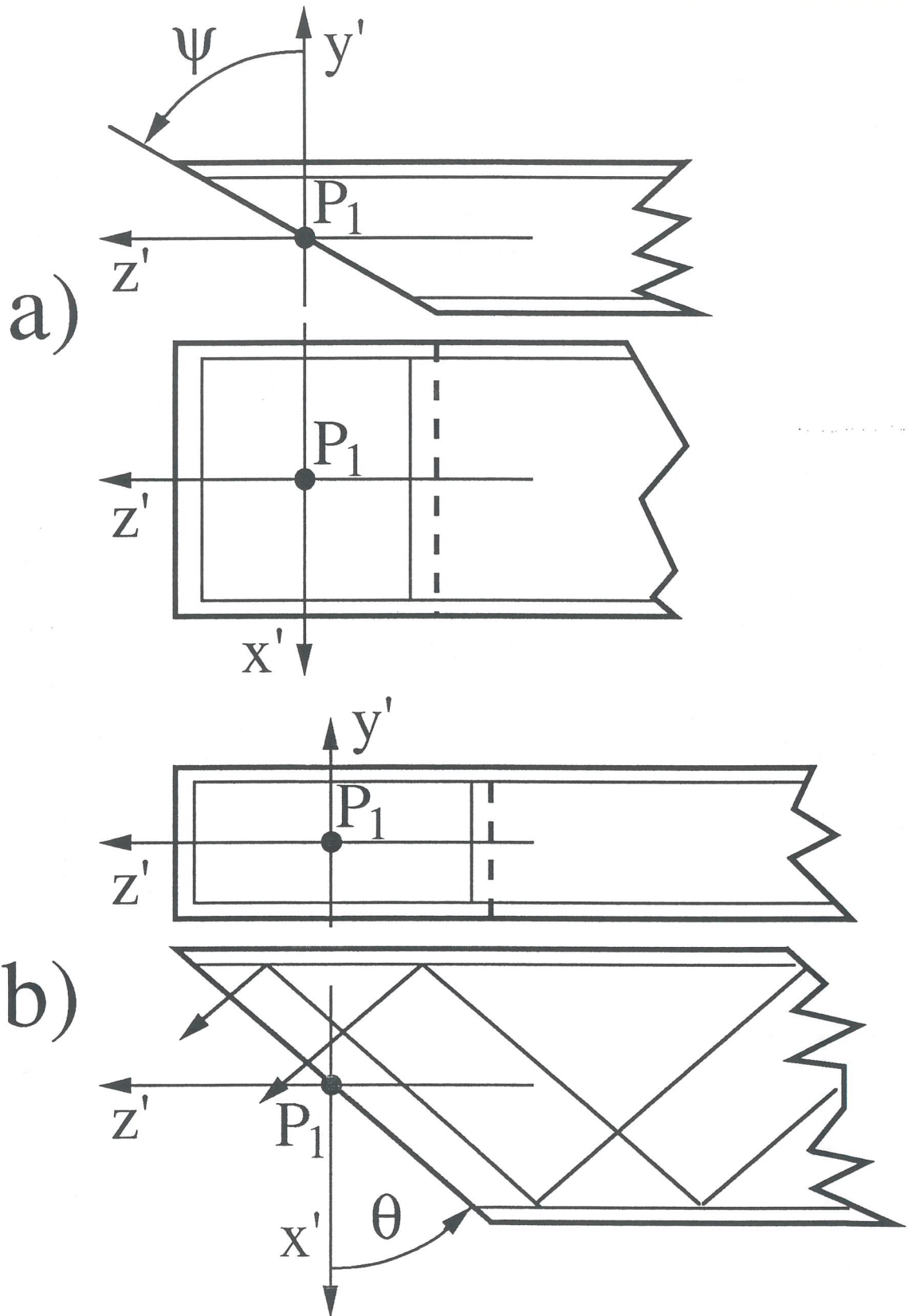
Fig 18) Cut planes for the couplers

Fig 19) Impedances and reflections as functions of plasma collision parameter. Lines are fit results
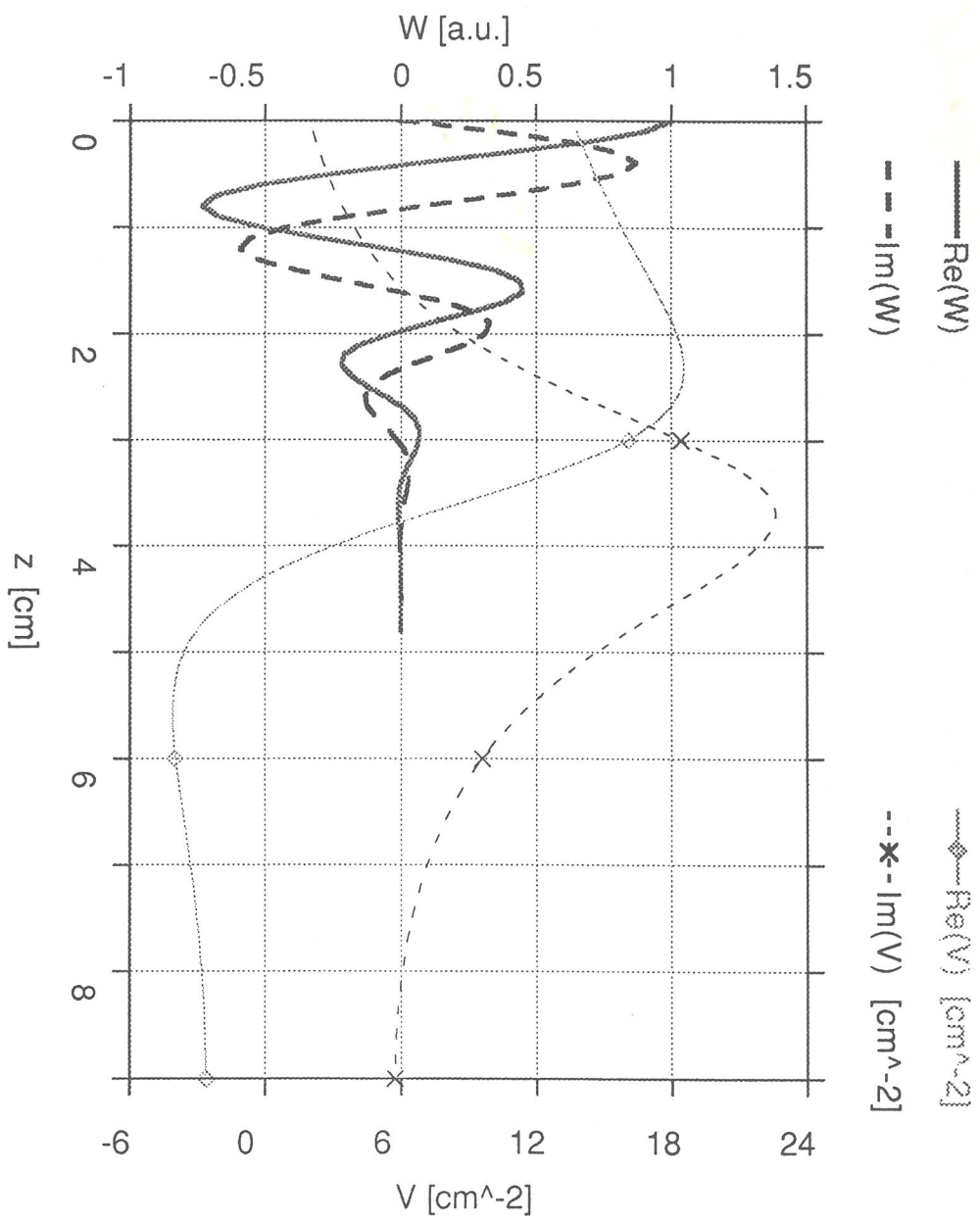
fig 20